JACC: BASIC TO TRANSLATIONAL SCIENCE VOL. 3, NO. 6, 2018
© 2018 THE AUTHORS. PUBLISHED BY ELSEVIER ON BEHALF OF THE AMERICAN COLLEGE OF CARDIOLOGY FOUNDATION. THIS IS AN OPEN ACCESS ARTICLE UNDER THE CC BY-NC-ND LICENSE (http://creativecommons.org/licenses/by-nc-nd/4.0/).

PRECLINICAL RESEARCH

Natriuretic Peptide Receptor-C Protects Against Angiotensin II-Mediated Sinoatrial Node Disease in Mice

Martin Mackasey, BSc,[a,b,*] Emmanuel E. Egom, MD, PhD,[b,*,†] Hailey J. Jansen, PhD,[a,b,*] Rui Hua, PhD,[b] Motahareh Moghtadaei, PhD,[b] Yingjie Liu, PhD,[a] Jaspreet Kaur, PhD,[a] Megan D. McRae, BHSc,[a] Oleg Bogachev, MD,[b] Sara A. Rafferty, MSc,[b] Gibanananda Ray, PhD,[b] Adam W. Kirkby, MSc,[a] Robert A. Rose, PhD[a,b]

VISUAL ABSTRACT

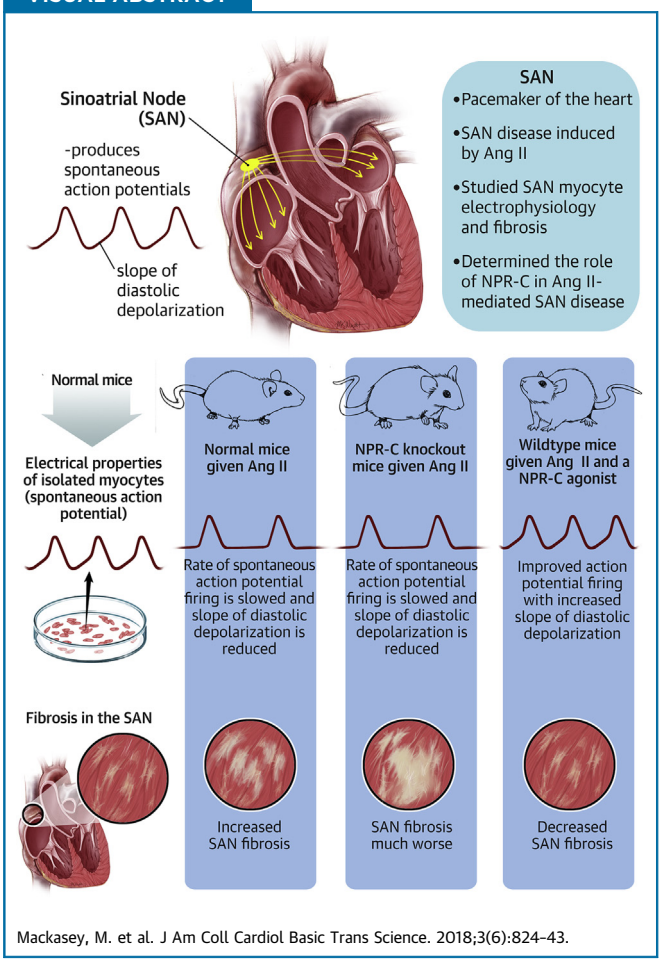

Mackasey, M. et al. J Am Coll Cardiol Basic Trans Science. 2018;3(6):824–43.

HIGHLIGHTS

- **Sinoatrial node (SAN) disease is prevalent in hypertension and heart failure and can be induced by chronic angiotensin II (Ang II) treatment in mice.**
- **Ang II caused SAN disease in mice in association with impaired electrical conduction, reduction in the hyperpolarization-activated current (I_f) in SAN myocytes, and increased SAN fibrosis.**
- **Ang II-induced SAN disease was worsened in mice lacking natriuretic peptide receptor C (NPR-C) in association with enhanced SAN fibrosis.**
- **Mice co-treated with Ang II and an NPR-C agonist (cANF) were protected from SAN disease.**
- **NPR-C may represent a new target to protect against Ang II-induced SAN disease.**

From the [a]Department of Cardiac Sciences, Libin Cardiovascular Institute of Alberta, Cumming School of Medicine, University of Calgary, Calgary, Alberta, Canada, and Department of Physiology and Pharmacology, Cumming School of Medicine, University of Calgary, Calgary, Alberta, Canada; and the [b]Department of Physiology and Biophysics, Faculty of Medicine, Dalhousie University, Halifax, Nova Scotia, Canada. Supported by Canadian Institutes of Health Research grants MOP 93718 and 142486 to Prof. Rose. Prof. Rose holds a New Investigator Award from the Heart and Stroke Foundation of Canada. Dr. Egom is an employee of ECTRS Ltd. Mr. Mackasey is the recipient of a Libin Cardiovascular Institute of Alberta graduate scholarship. Dr. Egom held a Heart and

ISSN 2452-302X https://doi.org/10.1016/j.jacbts.2018.08.004

SUMMARY

Sinoatrial node (SAN) disease mechanisms are poorly understood, and therapeutic options are limited. Natriuretic peptide(s) (NP) are cardioprotective hormones whose effects can be mediated partly by the NP receptor C (NPR-C). We investigated the role of NPR-C in angiotensin II (Ang II)-mediated SAN disease in mice. Ang II caused SAN disease due to impaired electrical activity in SAN myocytes and increased SAN fibrosis. Strikingly, Ang II treatment in NPR-$C^{-/-}$ mice worsened SAN disease, whereas co-treatment of wild-type mice with Ang II and a selective NPR-C agonist (cANF) prevented SAN dysfunction. NPR-C may represent a new target to protect against the development of Ang II-induced SAN disease. (J Am Coll Cardiol Basic Trans Science 2018;3:824–43)
© 2018 The Authors. Published by Elsevier on behalf of the American College of Cardiology Foundation. This is an open access article under the CC BY-NC-ND license (http://creativecommons.org/licenses/by-nc-nd/4.0/).

ABBREVIATIONS AND ACRONYMS

Ang II = angiotensin II
AP = action potential
cSNRT = corrected sinoatrial node recovery time
CV = conduction velocity
DD = diastolic depolarization
G_{max} = maximum conductance
HR = heart rate
$I_{Ca,L}$ = L-type calcium current
$I_{Ca,T}$ = T-type calcium current
I_f = hyperpolarization-activated current
I_{NCX} = sodium–calcium exchanger current
IV = current voltage relationship
NP = natriuretic peptide
NPR = natriuretic peptide receptor
NPR-C = natriuretic peptide receptor C
SAN = sinoatrial node
SBP = systolic blood pressure
$V_{1/2(act)}$ = voltage for 50% channel activation

Sinoatrial node (SAN) disease is a highly prevalent but poorly understood form of cardiovascular disease that occurs in a number of conditions including hypertension, hypertrophy, and heart failure (1–4). Arrhythmias associated with SAN dysfunction account for approximately 50% of sudden deaths in the hospital in heart failure patients (2,5). A common theme in these prevalent forms of cardiovascular disease is a pathological elevation in angiotensin II (Ang II) and enhanced Ang II signaling (6,7). SAN disease in hypertension and heart failure is characterized by sinus bradycardia and chronotropic incompetence due, at least in part, to the SAN's compromised ability to generate spontaneous action potentials (APs) and excite the surrounding atrial myocardium (5,8). Mechanisms responsible for SAN disease remain poorly understood, which severely limits therapeutic options. Currently, artificial pacemaker implantation is the major treatment approach for SAN disease; however, this comes with substantial costs and a number of patient risks, including infections, hematoma, pneumothorax, endocarditis, limited response to autonomic regulation, lead dislodgment, and lead failure. The burden of ongoing, lifelong complications from these devices, which can help sustain function but do affect underlying disease mechanisms, indicates a clear need for improved treatment options for patients with SAN disease.

Under normal conditions, the heart beat is initiated in the SAN due to the ability of this specialized region of the heart to generate spontaneous APs characterized by the presence of a diastolic depolarization (DD) (9,10). The DD is produced by a number of underlying ionic mechanisms including the hyperpolarization-activated current (I_f), T-type and L-type Ca^{2+} currents ($I_{Ca,T}$ and $I_{Ca,L}$, respectively), a Na^+-Ca^{2+} exchange current (I_{NCX}) driven by sarcoplasmic reticulum Ca^{2+} release, and repolarizing K^+ currents (9,11). Alterations in the activity and coordination of these currents can compromise SAN pacemaker activity. Pacemaker activity in the heart is also importantly affected by the amount of fibrosis in the SAN, and enhanced fibrosis can impair normal SAN function (6,12).

Natriuretic peptide(s) (NP) are a family of cardioprotective hormones with a number of effects in the cardiovascular system that are mediated by specific NP receptors called NPR-A, -B, and -C (13,14). Among this family, NPR-C remains the least understood. We have demonstrated that NPs have potent effects on cardiac electrophysiology, including in the SAN, and that some of these effects can be mediated by NPR-C (14–18). Furthermore, we have recently shown that NPR-C knockout (NPR-$C^{-/-}$) mice develop SAN dysfunction in association with enhanced fibrosis (19). These findings suggest that NPR-C plays an integral role in maintaining normal SAN structure and function and that it could be a novel therapeutic target; however, the role of NPR-C

Stroke Foundation of Canada fellowship. Dr. Jansen holds a Killam postdoctoral fellowship. Dr. Liu is the recipient of a Cumming School of Medicine postdoctoral scholarship. The other authors have reported that they have no industry relationships relevant to the contents of this paper to disclose. *Mr. Mackasey, Dr. Egom and Dr. Jansen contributed equally to this work and are joint first authors. †Present address: Department of Medicine, St. Martha's Regional Hospital, Antigonish, Nova Scotia, Canada.
All authors attest they are in compliance with human studies committees and animal welfare regulations of the authors' institutions and Food and Drug Administration guidelines, including patient consent where appropriate. For more information, visit the *JACC: Basic to Translational Science* author instructions page.

Manuscript received March 30, 2018; revised manuscript received August 15, 2018, accepted August 16, 2018.

in the SAN in cardiovascular disease remains unexplored.

This study used a mouse model of hypertension induced by chronic Ang II treatment to investigate the mechanisms for SAN disease in the setting of elevated Ang II and the role of NPR-C in the progression of SAN disease. Our studies demonstrate that chronic Ang II treatment causes SAN disease in association with electrical and structural remodeling. We also demonstrate that the progression of SAN disease is enhanced in the absence of NPR-C and that chronic NPR-C activation can prevent development of SAN disease.

METHODS

An expanded methods and materials section can be found in the Supplemental Material.

ANIMALS AND SURGICAL INTERVENTIONS. This study used male wild-type and NPR-C$^{-/-}$ mice between 10 and 15 weeks of age. NPR-C$^{-/-}$ mice were initially obtained from the Jackson Laboratory (strain B6;C-*Npr3lgj*/J; Bar Harbor, Maine) and backcrossed into the C57Bl/6 line as we previously reported (15,19,20). Mice of each genotype were treated with Ang II (3 mg/kg per day) or saline for 3 weeks, using osmotic minipumps (Alzet, Cupertino, California). In some cases, the NPR-C agonist [des(Gln^{18}, Ser^{19}, Gly^{20}, Leu^{21}, Gly^{22})ANP$_{4\text{-}23}$-NH$_2$]; cANF$_{4\text{-}23}$; catalog H-3134; Bachem, Torrance, California) was also delivered by osmotic minipump along with Ang II at doses of 0.07 or 0.14 mg/kg per day. cANF is a well-characterized NPR-C agonist that has no effects on the guanylyl cyclase-linked NPR-A and NPR-B receptors (13,16,21-23). Numbers of mice treated with cANF are noted in the relevant figure legends. To insert osmotic pumps, mice were anesthetized by isoflurane inhalation, and the pumps were inserted subcutaneously through a small midscapular incision. All experimental procedures were approved by the University of Calgary Animal Care and Use Committee and the Dalhousie University Committee for Laboratory Animals and were conducted in accordance with Canadian Council on Animal Care guidelines.

ECHOCARDIOGRAPHY AND SYSTOLIC BLOOD PRESSURE ASSESSMENT. Cardiac structure and function were assessed in anesthetized mice (isoflurane inhalation) by using transthoracic echocardiography at baseline and after 3 weeks of drug treatment. Echocardiography was performed using a high-resolution transducer and a Vivid 7 ultrasound machine (GE Healthcare, Laurel, Maryland) to measure 2-dimensional (2D) M-mode images from the parasternal short axis at the level of the midpapillary muscle, as we have described previously (19,24). Systolic blood pressure (SBP) was measured in conscious, restrained mice at baseline and after 3 weeks of drug treatment, using a tail cuff apparatus (IITC Life Sci, Woodland Hills, California).

IN VIVO ELECTROPHYSIOLOGY. Surface ECGs were measured in anesthetized mice (2% isoflurane inhalation) using 30-ga subdermal needle electrodes (Grass Technologies, West Warwick, Rhode Island). In conjunction, a 1.2-F octapolar electrophysiology catheter (Transonic, Ithaca, New York) was inserted into the right heart through an incision in the jugular vein and used to measure corrected sinoatrial node recovery time (cSNRT), as we have described previously (19,24,25). Data were acquired using a Gould ACQ-7700 amplifier and Ponemah physiology platform software (Data Sciences International, St. Paul, Minnesota). Additional details are available in the Supplemental Material.

HIGH-RESOLUTION OPTICAL MAPPING. To study activation patterns and electrical conduction in the right atrial posterior wall, high-resolution optical mapping was performed in isolated atrial preparations, using methods we have described in detail previously (17,19,24,25). Atrial preparations were immobilized using blebbistatin (1 μM) (26). Changes in fluorescence were captured using the voltage-sensitive dye Di-4-ANEPPS (10 μM) and a high-speed electron-multiplying charge-coupled device camera (Evolve 128 model; Photometrics, Tucson, Arizona) at ~900 fps. Spatial resolution was 45 × 45 μm/pixel. All experiments were performed at 35°C. Data were analyzed using customized software written in Matlab version 9.1 software (Mathworks, Natick, Massachusetts). Further details are available in the Supplemental Material.

PATCH CLAMPING IN ISOLATED SAN MYOCYTES. Single pacemaker myocytes from the SAN were isolated using procedures we have described previously (15,19). Spontaneous APs were recorded using the perforated patch clamp technique in current clamp mode, while I_f and $I_{Ca,L}$ were recorded in the whole-cell configuration in voltage clamp mode. Solutions and protocols for these measurements are described in detail in the Supplemental Material.

QUANTITATIVE POLYMERASE CHAIN REACTION. Quantitative gene expression in the SAN (or right and left atria) was performed using established techniques we have described previously (15,25). Genes of interest that were measured include *Npr1* (encodes NPR-A), *Npr2* (encodes NPR-B), *Npr3* (encodes NPR-C), *HCN1*, *HCN2*, *HCN4*, *SCN5a* (encodes NaV1.5), *GJC1* (encodes Cx45) and *GJA1* (encodes Cx43). *GAPDH* was

used as a reference gene based on its stable expression levels across treatment groups. Additional information is available in the in Supplemental Material.

WESTERN BLOTTING. For Western blotting, SAN samples were extracted from 2 mice and pooled for each experimental replicate in order to ensure sufficient protein (27). In some cases, Western blotting was also performed on right and left atrial samples ($n = 3$ for each region). Western blotting was used to measure the protein expression of NPR-A, NPR-B, NPR-C, and HCN4, as well as GAPDH as the control. Procedures for these experiments are provided in the Supplemental Material.

COLLAGEN STAINING AND IMMUNOHISTOCHEMISTRY. Fibrosis in the SAN was assessed using picrosirius red staining on paraffin-embedded sections (8 μm) through the SAN. Sections were cut perpendicularly to the crista terminalis, and the SAN region was confirmed by HCN4 immunostaining (28,29) in adjacent sections. The level of fibrosis was quantified using ImageJ software (U.S. National Institutes of Health, Bethesda, Maryland). Additional details are provided in the Supplemental Material.

STATISTICS. All data are means ± SEM. Data were analyzed using Student *t*-test or 1- or 2-way ANOVA with Tukey post hoc test as indicated in each figure legend. A p value <0.05 was considered significant. Statistical analysis was conducted using SigmaPlot version 11.0 software (Systat, San Jose, California). Sample sizes for each experimental approach ranged as follows: 11 to 17 mice/group for SBP analysis; 9 to 15 mice/group for echocardiography; 19 to 29 mice/group for intracardiac electrophysiology; 8 to 9 mice/group for autonomic blockade studies; 8 to 24 mice/group for optical mapping; 10 to 17 cells/group (minimum 5 mice/group) for patch clamping; 5 hearts/group for histology; 3 to 5 replicates/group for Western blotting; and 7 to 11 samples/group for quantitative polymerase chain reaction Specific numbers for all experiments conducted are noted in the figure legends.

RESULTS

EFFECTS OF ANG II ON SBP AND CARDIAC STRUCTURE IN WILDTYPE AND NPR-C$^{-/-}$ MICE. Initially we measured the effects of Ang II (or saline as a control) on SBP in wild-type and NPR-C knockout mice (Supplemental Figure S1). These data demonstrated that Ang II treatment increased ($p < 0.001$) SBP to very similar extents in wild-type and NPR-C$^{-/-}$ mice, such that there were no differences ($p = 0.115$) in the extent of hypertension between genotypes. There were also no differences ($p = 1.000$) in systolic pressure between wild-type and NPR-C$^{-/-}$ mice at baseline, as we have shown previously (19). As expected, saline treatment had no effect ($p = 1.000$) on systolic pressure.

Next, we used echocardiography to assess overall changes in cardiac structure and function in wild-type and NPR-C$^{-/-}$ mice treated with Ang II compared with saline controls. M-mode imaging of the left ventricle (Supplemental Figure S2, Supplemental Table S1) demonstrated that, in wild-type mice, Ang II treatment caused a hypertrophic response characterized by increases in thickness of the interventricular septum ($p < 0.001$) and in the left ventricular posterior wall ($p = 0.006$) and a reduction ($p < 0.001$) in left ventricular internal diameter. These structural changes occurred in association with modest increases in ejection fraction ($p = 0.007$) and fractional shortening ($p < 0.001$). These data indicate that Ang II treatment in wild-type mice caused concentric hypertrophy without compromising systolic performance. Strikingly, Ang II treatment in NPR-C$^{-/-}$ mice caused a much more severe response, despite the observation that there were no differences in ventricular structure and function between wild-type and NPR-C$^{-/-}$ mice at baseline. Specifically, Ang II treatment in NPR-C$^{-/-}$ mice caused ventricular dilation as indicated by an increase ($p = 0.004$) in left ventricular internal diameter and a tendency for the interventricular septum and the left ventricular posterior wall to be thinner. Furthermore, ejection fraction ($p < 0.001$) and fractional shortening ($p < 0.001$) were substantially reduced in NPR-C$^{-/-}$ mice treated with Ang II, indicating that, in contrast to wild-type mice, Ang II treatment in NPR-C$^{-/-}$ mice resulted in overt heart failure with ventricular dilation and impaired systolic function.

EFFECTS OF ANG II ON SAN FUNCTION IN WILD-TYPE AND NPR-C$^{-/-}$ MICE. Next, we used electrocardiography (ECG) recordings with intracardiac programmed stimulation to assess SAN function by measuring heart rate (HR) and corrected SAN recovery time (cSNRT) in anesthetized mice (**Figure 1A**). Ang II treatment reduced ($p < 0.001$) HR (**Figure 1B**) and prolonged ($p < 0.001$) cSNRT (**Figure 1C**) in wild-type and NPR-C$^{-/-}$ mice. Notably, following Ang II treatment, HR was lower ($p < 0.001$) and cSNRT was more severely prolonged ($p < 0.001$) in NPR-C$^{-/-}$ mice than in wild-types. SAN function was further assessed by measuring intrinsic HR in anesthetized mice after autonomic nervous system blockade with atropine (10 mg/kg) and propranolol (10 mg/kg) (Online Figure S3). These data demonstrated that intrinsic HR (i.e., SAN function) was reduced ($p < 0.001$)

print & web 4C/FPO

FIGURE 1 Assessment of Heart Rate and SAN Function in Wild-Type and NPR-C$^{-/-}$ Mice Treated With Ang II

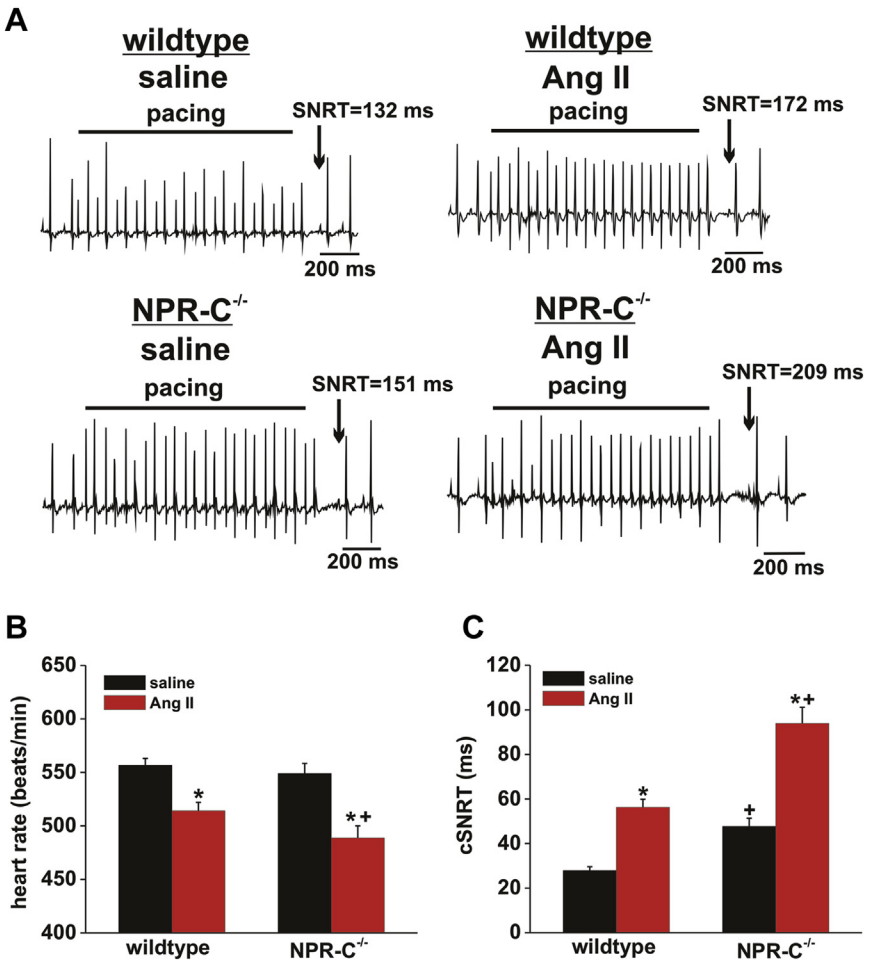

(A) Representative ECG recordings obtained during intracardiac programmed stimulation in anesthetized wild-type and NPR-C$^{-/-}$ mice treated with saline or Ang II to measure SNRT. **(B)** Summary of heart rate in wild-type and NPR-C$^{-/-}$ mice treated with saline or Ang II. **(C)** Summary of cSNRT in wild-type and NPR-C$^{-/-}$ mice treated with saline or Ang II. *p $<$ 0.001 versus saline; $^{+}$p $<$ 0.001 versus wild type by 2-way analysis of variance with Tukey post hoc test; n = 28 mice for wild-type/saline treatment, 29 mice for wild-type/Ang II treatment, 19 mice for NPR-C$^{-/-}$/saline treatment, and 19 mice for NPR-C$^{-/-}$/Ang II treatment. Ang II = angiotensin II; cSNRT = corrected SNRT; ECG = electrocardiography; NPR-C= natriuretic peptide receptor C; SAN = sinoatrial node; SNRT = sinoatrial node recovery time.

following Ang II treatment in wild-type and NPR-C$^{-/-}$ mice but that this reduction is larger, resulting in lower (p = 0.004) intrinsic HR in NPR-C$^{-/-}$ mice (Supplemental Figure S3B). Consistent with our prior studies (19), these data also demonstrated that cSNRT was longer (p $<$ 0.001) (**Figure 1C**) and intrinsic HR was lower (p = 0.037) (Supplemental Figure S3) in saline-treated NPR-C$^{-/-}$ mice than saline-treated wild types. These observations demonstrate that Ang II treatment induces SAN disease and that this is exacerbated in NPR-C$^{-/-}$ mice.

Conduction in the right atrial posterior wall following Ang II treatment was investigated using high-resolution optical mapping techniques, which we used previously (19,24,25). Activation maps, which were measured in the right atrial posterior wall adjacent to the crista terminalis (**Figure 2A**) in wild-type and NPR-C$^{-/-}$ mice treated with saline or Ang II, revealed distinct patterns in each group (**Figure 2B**). Specifically, these activation maps revealed that conduction time through the right atrial posterior wall adjacent to the crista terminalis was slowed in wild-type and in NPR-C$^{-/-}$ mice treated with Ang II compared with that in saline controls and that this slowing was greatest in NPR-C$^{-/-}$ mice. Furthermore, the hearts from mice treated with Ang II

print & web 4C/FPO

FIGURE 2 Assessment of Electrical Conduction in the SAN in Wild-Type and NPR-C$^{-/-}$ Mice Treated With Ang II

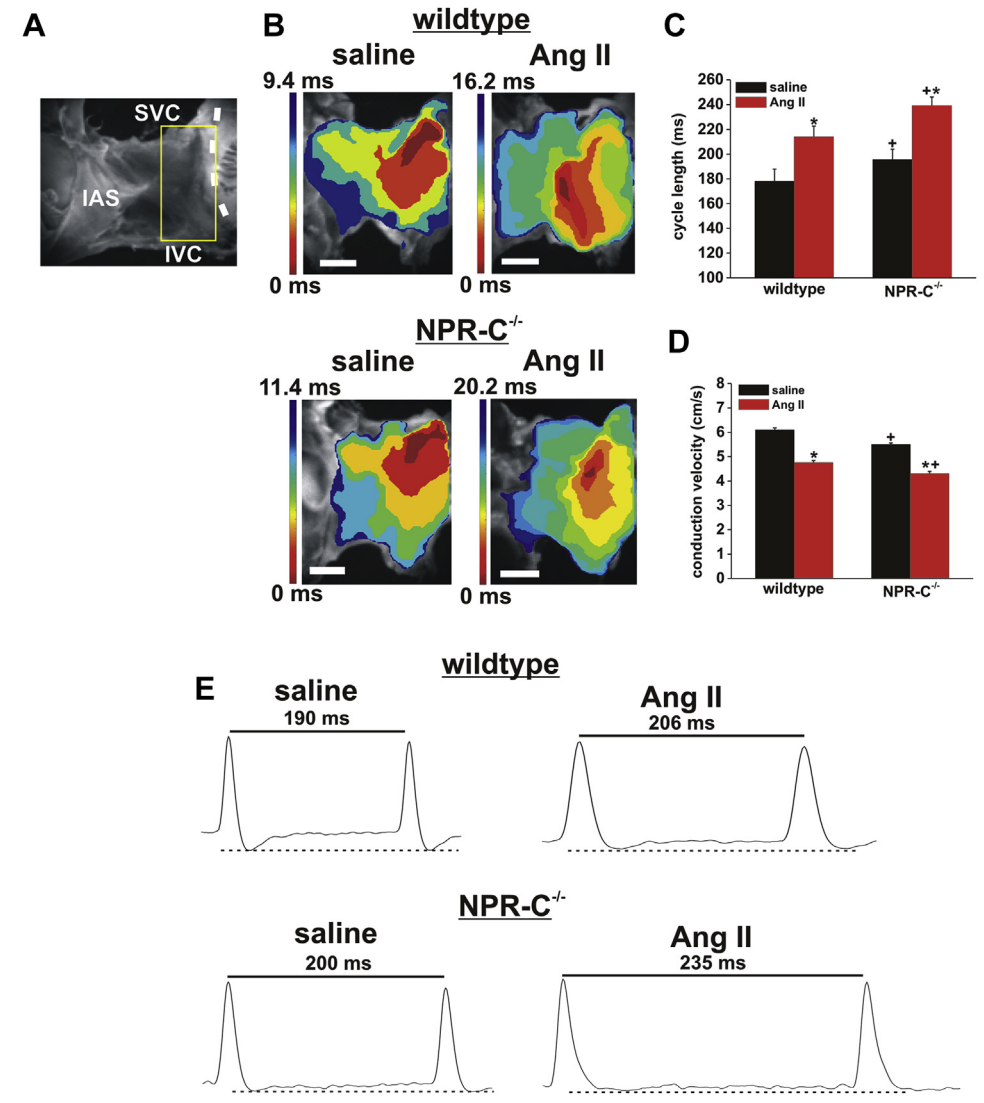

(A) Atrial preparation used in optical mapping. **Dashed line** indicates the location of the crista terminalis. The SAN is located in the intercaval region of the right atrial posterior wall adjacent to the crista terminals. The **yellow box** illustrates the area that was typically mapped. **(B)** Representative activation maps in atrial preparations from wild-type and NPR-C$^{-/-}$ mice treated with saline or Ang II. Bars = 1 mm. **(C)** Summary data for cycle length in wild-type and NPR-C$^{-/-}$ mice treated with saline or Ang II. *$p < 0.001$ versus saline; $^{+}p = 0.048$ versus wild type by 2-way analysis of variance (ANOVA) with Tukey post hoc test. **(D)** Summary data for SAN CV in wild-type and NPR-C$^{-/-}$ mice treated with saline or Ang II. *$p < 0.001$ versus saline; $^{+}p < 0.001$ versus wild type by 2-way ANOVA with Tukey post hoc test; n = 16 hearts for wild type/saline, 24 hearts for wild type/Ang II, 13 hearts for NPR-C$^{-/-}$/saline, and 12 hearts for NPR-C$^{-/-}$/Ang II. **(E)** Representative spontaneous SAN optical APs in wild-type and NPR-C$^{-/-}$ mice treated with saline or Ang II. **Dashed lines** run through the maximum diastolic potential. AP = action potential; CV = conduction velocity; IAS = interatrial septum; IVC = opening of inferior vena cava; SVC = opening of superior vena cava; other abbreviations as in Figure 1.

(wild type and NPR-C$^{-/-}$) displayed activation sites that were shifted inferiorly compared with those in saline-treated hearts.

We quantified cycle length and local conduction velocity (CV) within the right atrial posterior wall, using our previously established approaches (19,25). These data demonstrated that cycle length (Figure 2C) was prolonged ($p < 0.001$) by Ang II treatment in wild-type mice, further confirming impairment in SAN function. Cycle length was also prolonged ($p = 0.048$)

in saline-treated NPR-C$^{-/-}$ mice compared with that in wild-type controls, whereas Ang II treatment in NPR-C$^{-/-}$ mice resulted in the longest ($p = 0.048$) cycle lengths. As expected, CVs in this region of the heart were relatively low (i.e., less than 10 cm/s) (**Figure 2D**) (19,24). CV was reduced ($p < 0.001$) in wild-type mice treated with Ang II and was also lower ($p < 0.001$) in NPR-C$^{-/-}$ mice treated with saline than in wild-type controls. Ang II treatment in NPR-C$^{-/-}$ mice resulted in substantial slowing of CV in the right atrial posterior wall, which was lower ($p < 0.001$) than that in Ang II-treated wild-type mice.

Optical APs from the pacemaker region of the right atrial posterior wall demonstrated the changes in cycle length, as well as alterations in AP morphology, in these treatment groups. Specifically, representative optical APs (**Figure 2E**) showed that wild-type mice treated with saline have the shortest cycle lengths (i.e., faster frequency of spontaneous AP firing) and a robust DD. Ang II treatment prolonged the cycle length between successive APs and reduced the slope of the DD in wild-type mice. AP cycle length was also increased in saline-treated NPR-C$^{-/-}$ mice, which is consistent with our prior work (19). Finally, Ang II-treated NPR-C$^{-/-}$ mice exhibited the longest intrinsic AP cycle length and a clear reduction in DD slope. The properties of SAN APs were further investigated in isolated cells as described subsequently.

ANG II CAUSES ELECTRICAL REMODELING IN SAN MYOCYTES. To further investigate the effects of Ang II on SAN AP firing, we measured spontaneous APs in isolated SAN myocytes from wild-type and NPR-C$^{-/-}$ mice treated with saline or Ang II (**Figure 3A**; Supplemental Table S2). Summary data demonstrated that Ang II treatment increased ($p < 0.001$) AP cycle length (i.e., slowed AP frequency) (**Figure 3B**) in association with a reduction ($p < 0.001$) in DD slope (**Figure 3C**) in wild-type and NPR-C$^{-/-}$ mice. Interestingly, in contrast to our findings in intact atrial preparations, there were no differences in AP cycle length ($p = 0.557$) or DD slope ($p = 0.517$) between genotypes following saline or Ang II treatment in isolated SAN myocytes.

The ionic basis for these alterations in SAN AP morphology was investigated next. First, we measured the hyperpolarization-activated current (I_f) in SAN myocytes isolated from saline- and Ang II-treated wild-type and NPR-C$^{-/-}$ mice (**Figure 3D**). I_f IV curves for wild-type mice (**Figure 3E**) and NPR-C$^{-/-}$ mice (**Figure 3F**) demonstrate that Ang II reduced I_f density ($p < 0.001$) similarly in both genotypes. Analysis of I_f activation kinetics (**Figures 3G and 3H**; Supplemental Figure S4) revealed that the voltage for 50% channel activation ($V_{1/2(act)}$) was not affected by Ang II ($p = 0.416$) and not different between genotypes ($p = 0.361$). Similarly, the slope factor (k) for the I_f activation curves was not affected by Ang II ($p = 0.057$) or genotype ($p = 0.061$).

A reduction in I_f density without changes in activation kinetics suggests the current is reduced due to changes in ion channel expression. Accordingly, we next measured the mRNA expression level of the major *HCN4* channel isoforms in the SAN of wild-type mice treated with saline or Ang II (Supplemental Figure S5). *HCN4*, which is a major *HCN4* isoform in the mouse, was measured in the SAN as well as the right and left atria to ensure specificity of our SAN samples (Supplemental Figure S5A). From these data, it was apparent that our SAN samples expressed *HCN4* highly and that *HCN4* levels were very low or negligible in the right and left atria. Furthermore, *HCN4* mRNA expression was reduced ($p < 0.001$) specifically in the SAN but not in the right ($p = 0.676$) or left ($p = 0.984$) atrium after Ang II treatment. *HCN1* and *HCN2* levels were measured in these same SAN samples. These data demonstrated that *HCN1* ($p = 0.517$) (Supplemental Figure S5B) and *HCN2* ($p = 0.067$) (Supplemental Figure S5C) mRNA expression levels were not altered in the SAN of Ang II-treated mice.

HCN4 expression level in the SAN was also measured by Western blotting (Supplemental Figure S5D). Once again, we first confirmed that SAN samples used for Western blotting expressed HCN4 protein highly compared with that in the right and left atria where HCN4 protein expression was negligible (Supplemental Figure S5D). We then measured the expression level of HCN4 protein in the SAN of saline- and Ang II-treated mice. These measurements confirmed that Ang II treatment caused a reduction ($p = 0.044$) in HCN4 protein in the SAN (Supplemental Figure S5E).

We also measured $I_{Ca,L}$, as carried by channels $Ca_V1.2$ and $Ca_V1.3$ (15,30,31), in SAN myocytes from wild-type mice treated with saline or Ang II (Supplemental Figure S6A). The $I_{Ca,L}$ IV curves (Supplemental Figure S6B) demonstrate no differences ($p = 0.503$) in $I_{Ca,L}$ density between treatment groups. Similarly, analysis of $I_{Ca,L}$ activation kinetics (Supplemental Figure 6C) shows that $I_{Ca,L}$ maximum conductance (G_{max}, $p = 0.877$) (Supplemental Figure S6D), $V_{1/2(act)}$ ($p = 0.342$, Supplemental Figure 6E), and slope factor (k, $p = 0.270$) (Online Figure S6F) were not affected by Ang II treatment.

Finally, we performed additional gene expression studies to assess whether there were additional contributors to impaired electrical function in the SAN following Ang II treatment. Specifically, we measured

print & web 4C/FPO

FIGURE 3 Effects of Ang II on AP Morphology and Hyperpolarization-Activated Current (I_f) in Isolated SAN Myocytes From Wild-Type and NPR-$C^{-/-}$ Mice

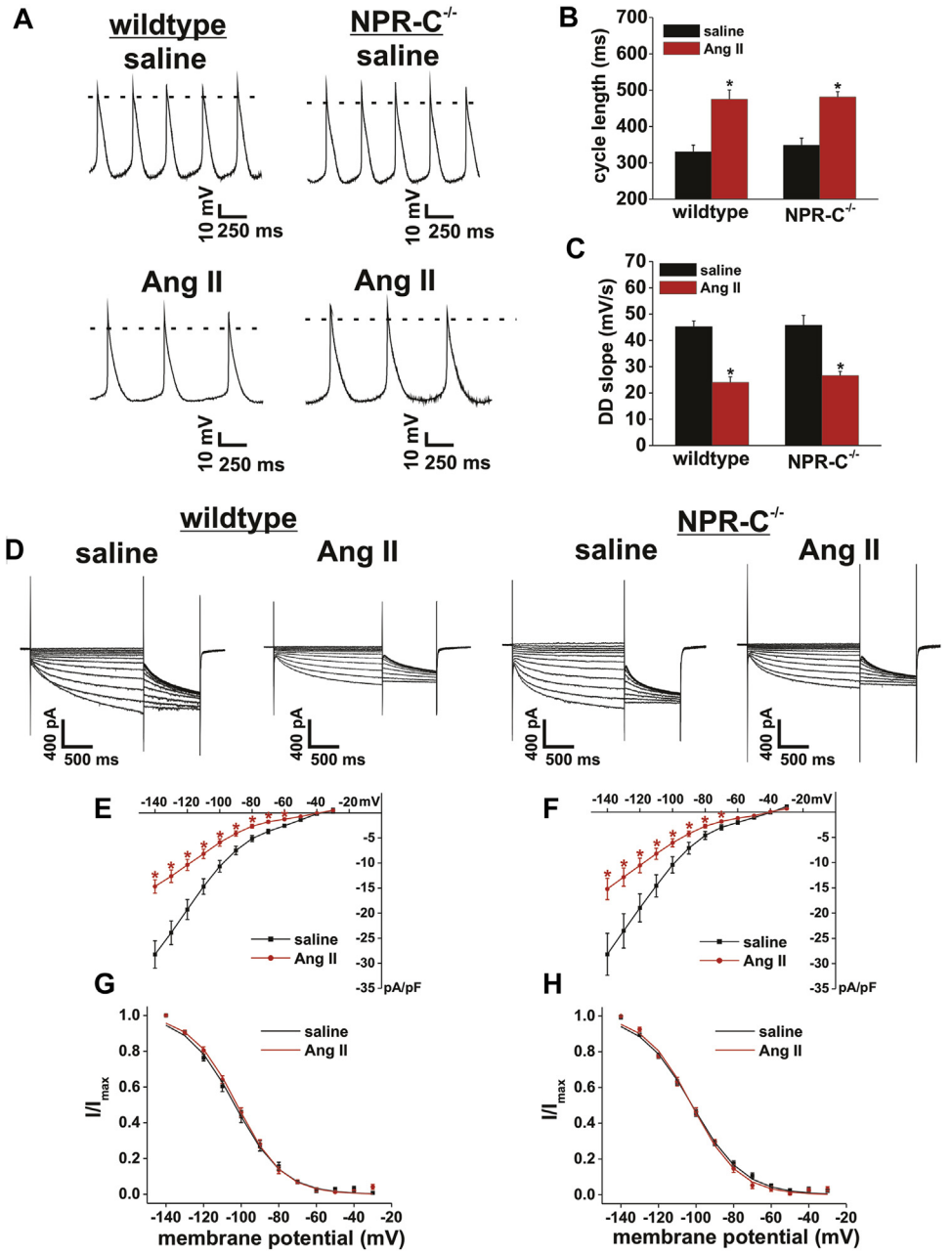

(A) Representative spontaneous AP recordings in wild-type and NPR-$C^{-/-}$ SAN myocytes treated with saline or Ang II. **(B) (C)** Summary data illustrating cycle length **(B)** and DD slope **(C)** in wild-type and NPR-$C^{-/-}$ mice treated with saline or Ang II. *$p < 0.001$ versus saline; $p = 0.557$ for AP cycle length and $p = 0.517$ for DD slope between genotypes within treatment group; $n = 16$ cells for wild type/saline, 11 cells for wild type/Ang II, 10 cells for NPR-$C^{-/-}$/saline, and 13 cells for NPR-$C^{-/-}$/Ang II for AP data. See Supplemental Table S2 for additional AP parameters. **(D)** Representative I_f recordings in SAN myocytes isolated from wild-type and NPR-$C^{-/-}$ mice treated with saline or Ang II. **(E) (F)** Summary I_f IV curves for wild-type **(E)** and NPR-$C^{-/-}$ **(F)** mice treated with saline or Ang II. *$p < 0.001$ versus saline at each membrane potential by 2-way repeated-measures analysis of variance with Tukey post-hoc test. **(G) (H)** I_f activation curves for wild-type **(G)** mice and NPR-$C^{-/-}$ **(H)** mice treated with Ang II. See Supplemental Figure S4 for additional I_f kinetic analysis. $n = 17$ cells for wild type/saline, 13 cells for wild type/Ang II; 13 cells for NPR-$C^{-/-}$/saline, and 16 cells for NPR-$C^{-/-}$/Ang II. IV = current voltage relationship; pA = picoamperes; pF = picofarads; other abbreviations as in **Figures 1 and 2**.

the mRNA expression levels of *SCN5a* (encodes $Na_V1.5$ and has been shown to contribute to SAN conduction) (32); *GJC1* (Cx45), a major connexin in the SAN (33); and *GJA1* (Cx43), which can be detected at the mRNA in the SAN (34,35). These data demonstrated that there were no differences in the expression levels of SCN5a ($p = 0.335$) (Supplemental Figure S7A) or *GCJ1* ($p = 0.680$) (Supplemental Figure S7B) in the SAN of Ang II-treated mice. *GJA1* showed a modest reduction ($p = 0.002$) (Supplemental Figure S7C) in the SAN, although Cx43 was not thought to be a major contributor to SAN function (see the Discussion section).

ANG II CAUSES STRUCTURAL REMODELING IN THE SAN. The findings summarized in the preceding text demonstrate that SAN dysfunction following Ang II treatment occurred in association with impairments in spontaneous AP firing and reduced I_f. Notably, although the changes in AP cycle length and SAN conduction in NPR-$C^{-/-}$ mice treated with Ang II were greater than those in wild-type mice when measured in the intact atria, the impairments in AP firing (and I_f) elicited by Ang II were similar between wild-type and NPR-$C^{-/-}$ mice in isolated SAN myocytes. Thus, the ionic alterations in SAN myocytes do not explain the more severe progression of SAN dysfunction in NPR-$C^{-/-}$ mice.

Accordingly, the basis for SAN dysfunction following Ang II treatment was further investigated by measuring the level of fibrosis in the SAN. This was done using picrosirius red staining in histological sections taken from wild-type and NPR-$C^{-/-}$ mice treated with saline or Ang II. Sections were cut perpendicularly to the crista terminals, and adjacent sections were immunostained for HCN4. Representative images for each treatment group demonstrate HCN4-positive regions in the SAN in the first image and picrosirius red staining in the second image (**Figure 4A**). SAN fibrosis was assessed specifically within regions that aligned with the HCN4-positive zone. These representative images and the summary data (**Figure 4B**) demonstrated that Ang II treatment increased ($p < 0.001$) SAN fibrosis in wild-type and NPR-$C^{-/-}$ mice. Strikingly, the amount of SAN fibrosis was higher ($p = 0.014$) in NPR-$C^{-/-}$ mice than in wild types. Ang II-treated NPR-$C^{-/-}$ mice had substantially higher ($p = 0.014$) SAN fibrosis than Ang II-treated wild-type mice.

EFFECTS OF NPR-C ACTIVATION ON SBP AND CARDIAC FUNCTION. Results of experiments presented to this point demonstrated that Ang II causes SAN dysfunction in association with impairments in SAN electrical conduction and spontaneous AP firing as well as SAN fibrosis. Our data also demonstrated that Ang II treatment in the absence of NPR-C receptors exacerbates the progression to systolic heart failure and worsens SAN dysfunction, suggesting that NPR-C plays a central role in the progression of Ang II-mediated heart disease, including in the SAN.

To further test this hypothesis, we conducted a series of experiments in which wild-type mice were co-treated with Ang II and the selective NPR-C agonist cANF (21,22,36) at 2 different dosages (0.07 and 0.14 mg/kg per day). These dosages were selected to be comparable to those in other studies that administered NPs clinically and in animal studies (37–39). Initially we measured mRNA (Supplemental Figure S8A) and protein (Supplemental Figures S8B and S8C) expression for all 3 NPRs in the SAN of wild-type mice treated with saline or Ang II to determine whether NP receptor expression in the SAN was altered during chronic Ang II treatment. Ang II had no effects on the expression of NPR-A, -B, or -C in the SAN. We also measured SBP in mice treated with saline, Ang II, or Ang II plus cANF (both doses). These data (Supplemental Figure S9) demonstrated that SBP was elevated ($p < 0.001$) in mice treated with Ang II and in Ang II plus cANF. There were no differences in SBP between Ang II alone and Ang II plus cANF at dosages of 0.07 ($p = 0.859$) or 0.14 mg/kg per day ($p = 0.740$), indicating that cANF co-treatment did not prevent Ang II hypertension.

Next, we used echocardiography to determine the effects of cANF co-treatment on cardiac structure and function. M-mode images (Supplemental Figure S10) and summary data (Supplemental Table S3) demonstrated both dosages of cANF prevented the development of ventricular hypertrophy elicited by Ang II alone.

cANF PREVENTS DEVELOPMENT OF ANG II-MEDIATED SAN DYSFUNCTION. Using intracardiac electrophysiology in anesthetized mice, we measured the effects of co-treatment with Ang II and cANF on HR and SAN function (**Figure 5A**). Summary data illustrated that the lower dosage of cANF (0.07 mg/kg per day) did not prevent Ang II-mediated changes in HR ($p = 0.915$) (**Figure 5B**); however, there was a clear trend toward a reduction in cSNRT ($p = 0.067$) (**Figure 5C**) compared with Ang II alone. Furthermore, co-treatment with a higher dosage of cANF (0.14 mg/kg per day) potently prevented the reduction in HR ($p = 0.009$) and prolongation in cSNRT ($p < 0.001$) elicited by Ang II alone, such that HR ($p = 0.915$) and cSNRT ($p = 0.580$) were not different from those in saline controls (**Figures 5B and 5C**).

print & web 4C/FPO

FIGURE 4 Effects of Ang II on Interstitial Fibrosis in the SAN of Wild-Type and NPR-C$^{-/-}$ Mice

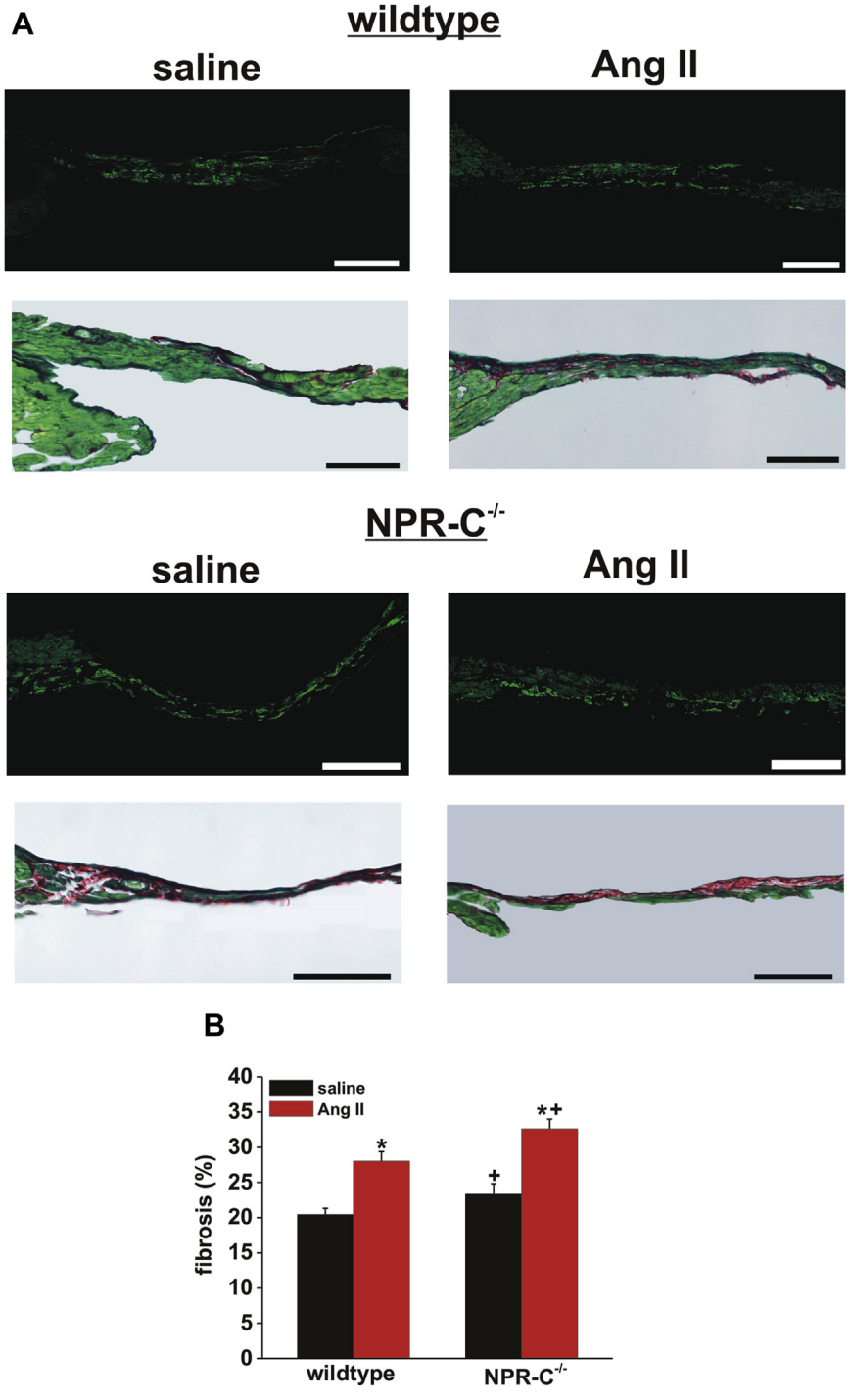

(A) Sections through the SAN in wild-type and NPR-C$^{-/-}$ mice treated with saline or Ang II. For each treatment group, the **top image** illustrates the HCN4-positive zone **(green)** used to identify the SAN region, and the **bottom image** illustrates the **picrosirius red** staining from an adjacent section used to identify fibrosis **(red)**. Bars = 50 μM. **(B)** Summary of SAN fibrosis measured in the HCN4-positive zone for wild-type and NPR-C$^{-/-}$ mice treated with saline or Ang II. *$p < 0.001$ versus saline; $^{+}p = 0.014$ versus wild type by 2-way analysis of variance with Tukey post hoc test; $n = 5$ hearts for each group.

print & web 4C/FPO

FIGURE 5 Assessment of Heart Rate and SAN Function in Wild-Type Mice Co-Treated With Ang II and the NPR-C Agonist cANF

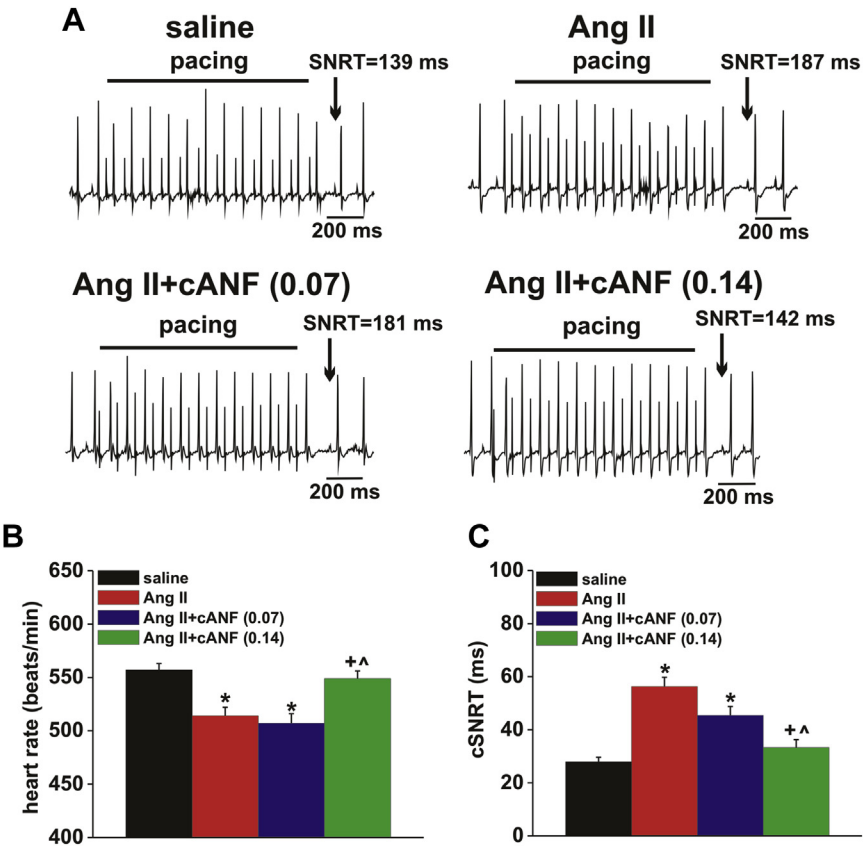

(A) Representative ECG recordings and SNRT measurements during intracardiac programmed stimulation in wild-type mice treated with saline, Ang II. or Ang II plus cANF (0.07 or 0.14 mg/kg per day). **(B) (C)** Summary of heart rate **(B)** and cSNRT **(C)** in wild-type mice treated with saline, Ang II, or Ang II plus cANF (0.07 or 0.14 mg/kg per day). **(B)** *$p < 0.001$ versus saline; $^{+}p = 0.009$ versus Ang II; $^{\wedge}p = 0.006$ versus Ang II plus cANF (0.07). **(C)** *$p < 0.001$ versus saline; $^{+}p < 0.001$ versus Ang II; $^{\wedge}p = 0.006$ versus Ang II plus cANF (0.07). Data were analyzed by one-way analysis of variance with Tukey post hoc test; $n = 28$ mice for saline, 29 mice for Ang II, 20 mice for Ang II plus cANF (0.07 mg/kg per day) and 22 mice for Ang II plus cANF (0.14 mg/kg per day). cANF = NPR-C agonist; other abbreviations as in Figure 1.

Similar effects of cANF co-treatment were observed using high-resolution optical mapping of the right atrial posterior wall (Figure 6). Specifically, representative activation maps (Figure 6A) demonstrate that conduction in the right atrial posterior wall was faster in atrial preparations from mice co-treated with cANF than with Ang II alone and that cANF co-treatment resulted in leading activation sites that were shifted back toward the superior portion of the right atrial posterior wall. Cycle length in atrial preparations from mice co-treated with the lower dose of cANF tended to be shorter than Ang II alone, whereas the higher dosage of cANF reduced ($p < 0.001$) cycle length to values that were not different ($p = 0.641$) from saline controls (Figure 6B). Furthermore, CV in the right atrial posterior wall following treatment with the low dosage of cANF tended to be higher than that of Ang II alone, but this did not reach statistical significance. CV was increased ($p < 0.001$) following co-treatment with the higher dose of cANF compared with that in Ang II alone to values that were not different from saline controls (Figure 6C). Optical APs further demonstrated that cANF dosage dependently shortened AP cycle length and increased the DD slope compared to those with Ang II alone (Figure 6D). These findings demonstrated that activation of NPR-C with cANF can dose-dependently prevent the development of SAN dysfunction elicited by Ang II.

EFFECTS OF cANF ON SAN MYOCYTE ELECTROPHYSIOLOGY AND FIBROSIS. To determine the mechanism(s) for the protective effects of NPR-C activation in the SAN during Ang II treatment, we

print & web 4C/FPO

FIGURE 6 Assessment of Electrical Conduction in the SAN in Wild-Type Mice Co-Treated With Ang II and the NPR-C Agonist cANF

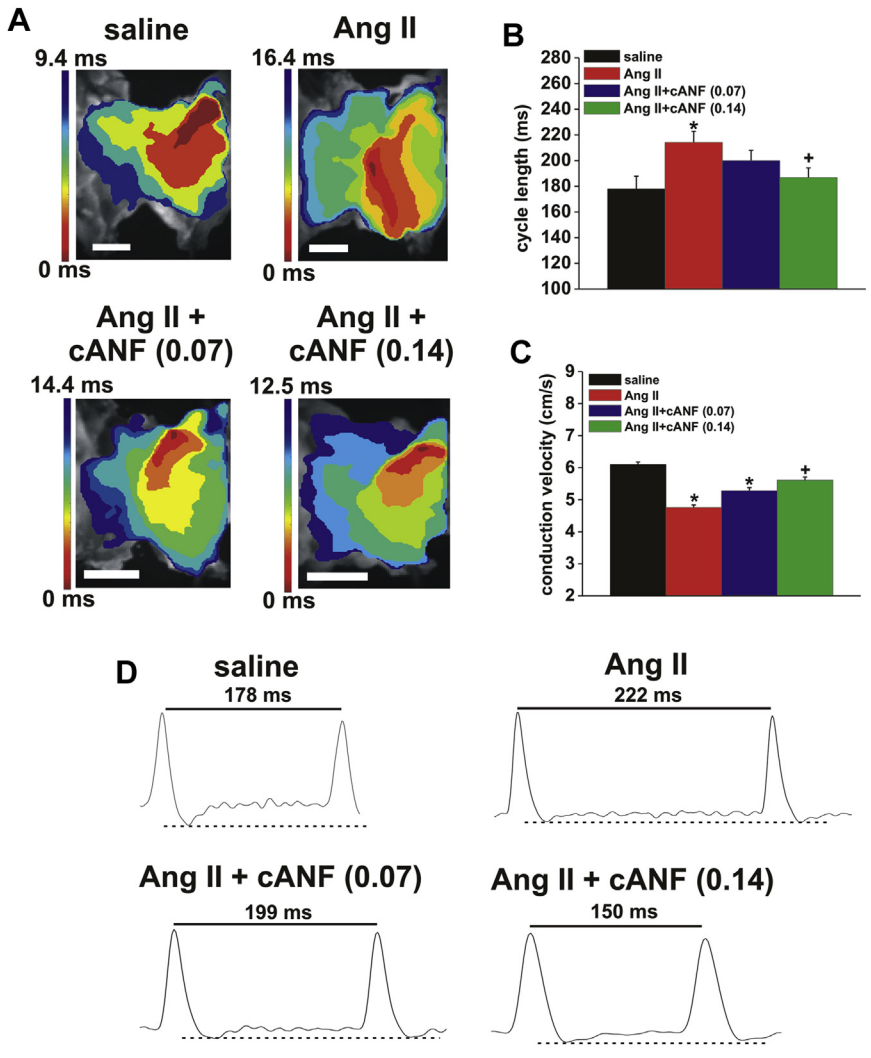

(A) Maps show wild-type mice treated with saline, Ang II, or Ang II plus cANF (0.07 or 0.14 mg/kg per day). **(B) (C)** Summary data for cycle length **(B)** and SAN CV **(C)** in wild-type mice treated with saline, Ang II, or Ang II plus cANF (0.07 or 0.14 mg/kg per day). **(B)** *$p = 0.013$ versus saline; $^{+}p < 0.001$ versus Ang II. **(C)** *$p < 0.001$ versus saline; $^{+}p < 0.001$ versus Ang II. Data were analyzed by one-way analysis of variance with Tukey post hoc test; $n = 16$ hearts for saline, 24 hearts for Ang II, 8 hearts for Ang II + cANF (0.07 mg/kg per day), and 8 hearts for Ang II plus cANF (0.14 mg/kg per day). **(D)** Representative spontaneous SAN optical APs in wild-type mice treated with saline, Ang II, or Ang II plus cANF (0.07 or 0.14 mg/kg per day). **Dashed lines** run through the maximum diastolic potential. Abbreviations as in **Figures 1, 2, and 5**.

measured spontaneous APs in SAN myocytes isolated from mice co-treated with cANF (**Figure 7A**; Supplemental Table S4). Summary data demonstrate that cANF dose-dependently prevented the increase in AP cycle length (i.e., prevented the slowing of AP firing) (**Figure 7B**) and the reduction in DD slope (**Figure 7C**). Specifically, the lower dosage of cANF had an intermediate effect such that AP cycle length was lower ($p < 0.046$) than that of Ang II alone but still longer ($p = 0.006$) than in saline-treated mice. In contrast, the higher dose of cANF reduced ($p = 0.008$) AP cycle length compared with Ang II alone, such that cycle length was not different ($p = 0.573$) from that in saline-treated mice. Very similar effects were seen for DD slope.

Consistent with these effects on AP morphology, cANF also dose-dependently prevented the reduction in I_f elicited by Ang II in SAN myocytes (**Figure 7D**).

print & web 4C/FPO

FIGURE 7 Effects of the NPR-C Activator cANF on Ang II-Mediated Alterations in AP Morphology and Hyperpolarization-Activated Current (I_f) in Isolated SAN Myocytes

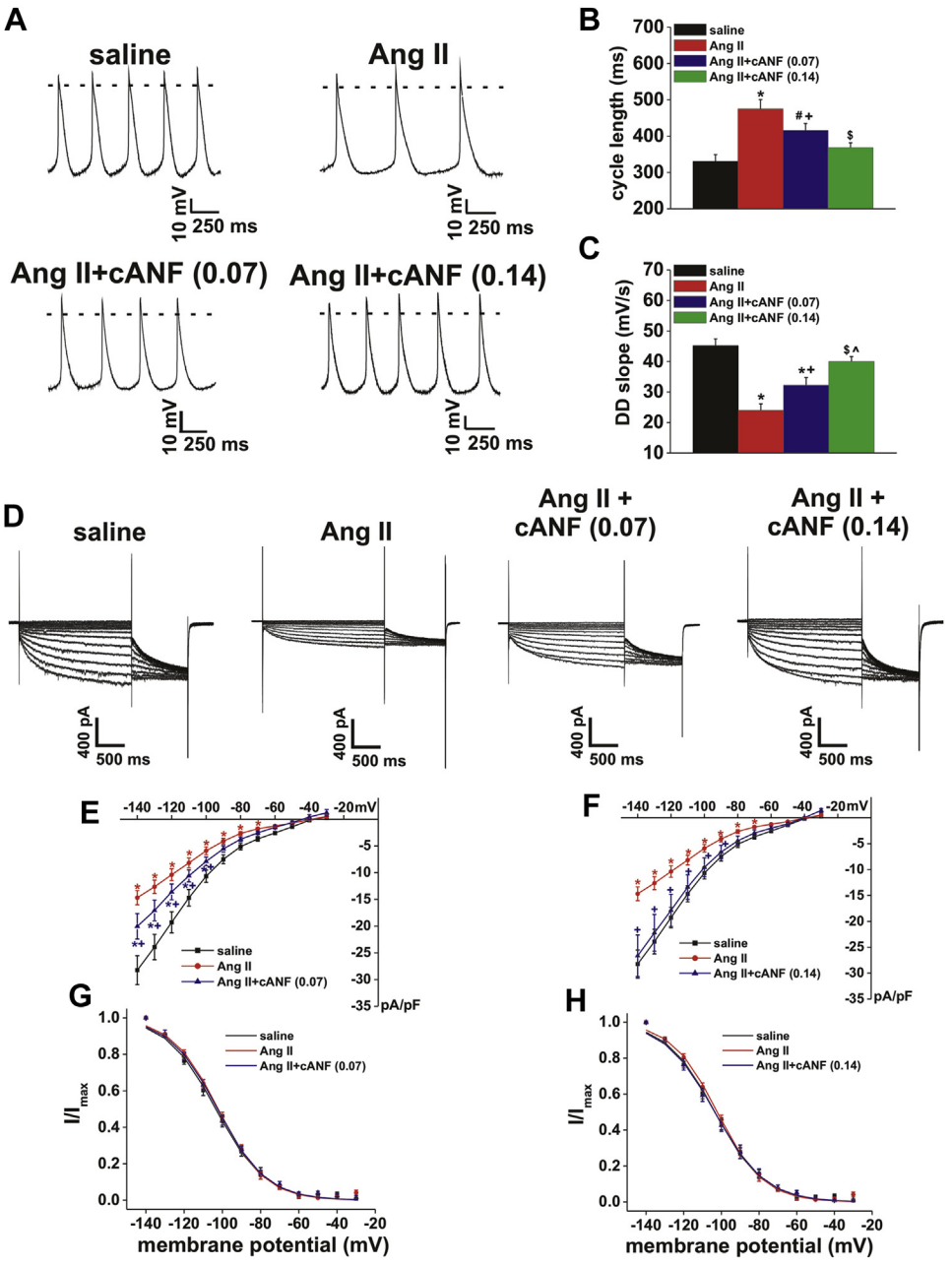

(A) Representative spontaneous AP recordings obtained in wild-type mice treated with saline, Ang II, or Ang II plus cANF (0.07 or 0.14 mg/kg per day). **(B) (C)** Summary of cycle length **(B)** and DD slope **(C)** illustrate the effects of cANF co-treatment on Ang II-mediated changes in SAN AP morphology. **(B)** *$p < 0.001$ versus saline; #$p = 0.006$ versus saline; +$p = 0.046$ versus Ang II; $$p = 0.008$ versus Ang II. **(C)** *$p < 0.001$ versus saline; +$p = 0.014$ versus Ang II; $$p < 0.001$ versus Ang II; ^$p = 0.024$ versus Ang II plus cANF (0.07). Data were analyzed by 1-way analysis of variance with Tukey post hoc test; n = 16 saline, 11 Ang II, 13 Ang II plus cANF (0.07), and 10 Ang II plus cANF (0.14) for AP data. See Supplemental Table S4 for additional AP parameters. **(D)** Representative I_f recordings from wild-type mice treated with saline, Ang II, or Ang II plus cANF (0.07 or 0.14 mg/kg per day). **(E) (F)** Summary IV curves for the effects of Ang II and cANF (0.07 and 0.14 mg/kg per day) on I_f. **(G) (H)** I_f activation curves illustrating the effects of Ang II and cANF (0.07 and 0.14 mg/kg per day) in SAN myocytes. **(E)** *$p < 0.001$ versus saline; +$p = 0.002$ versus Ang II. **(F)** *$p < 0.001$ versus saline; +$p < 0.001$ versus Ang II. Data were analyzed by 2-way repeated-measures analysis of variance with Tukey post hoc test; n = 17 cells for saline, 13 cells for Ang II, 14 cells for Ang II+cANF (0.07), and 13 cells for Ang II plus cANF (0.14). See Supplemental Figure S10 for additional I_f kinetic analysis. Abbreviations as in **Figures 1, 2, 3, and 5**.

print & web 4C/FPO

FIGURE 8 Effects of the NPR-C Agonist cANF on Ang II-Mediated Alterations in SAN Fibrosis

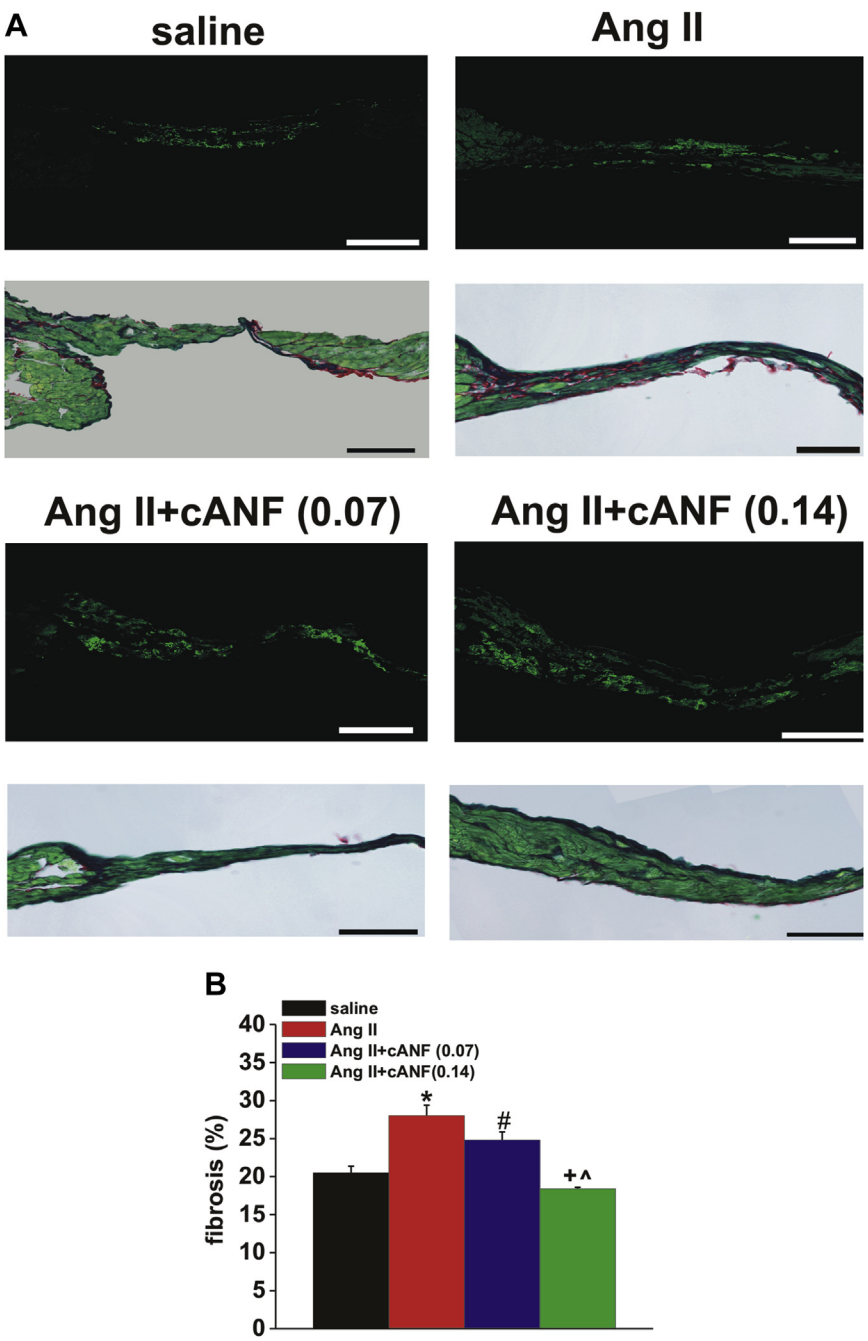

(A) SAN immunohistochemistry for HCN4 **(top)** and **picrosirius red** staining of fibrosis **(bottom)** for wild-type mice treated with saline, Ang II, or Ang II plus cANF (0.07 or 0.14 mg/kg per day). Bars = 50 μM. **(B)** Summary of the effects of cANF on Ang II-mediated fibrosis in the SAN. *$p < 0.001$ versus saline; #$p = 0.037$ versus saline; +$p < 0.001$ versus Ang II; ^$p = 0.004$ versus Ang II plus cANF (0.07) by one-way analysis of variance with Tukey post hoc test; n = 5 hearts for each group.

Once again, the lower dose of cANF had an intermediate effect, such that I_f density was larger ($p = 0.002$) than that in SAN myocytes treated with Ang II alone but still reduced ($p < 0.001$) compared with that in saline-treated SAN myocytes (Figure 7E). Co-treatment with the higher dosage of cANF fully prevented the reduction in I_f whereby I_f density was larger ($p < 0.001$) than Ang II alone and not different

($p = 0.441$) from that in saline-treated SAN myocytes (**Figure 7F**). In agreement with the results presented earlier (**Figure 3**), neither Ang II or cANF (with either dose) had any effects on I_f activation kinetics (**Figures 7G and 7H**; Supplemental Figure S11).

Finally, we assessed the effects of cANF co-treatment on fibrosis in the SAN by using picrosirius red staining and HCN4 immunostaining (**Figure 8**). These data demonstrate that the lower dose of cANF resulted in an intermediate level of SAN fibrosis that was still higher ($p = 0.037$) than that in saline-treated mice. In contrast, co-treatment with the higher dose of cANF potently prevented the increase in SAN fibrosis. Specifically, fibrosis in the SAN following the higher dose of cANF was reduced compared with that of Ang II alone ($p < 0.001$) and to that with the lower dose of cANF ($p = 0.004$) and not different ($p = 0.534$) from that of saline. Collectively, these findings demonstrate that selective NPR-C activation dose-dependently prevents Ang II-mediated impairments in SAN AP firing, the reduction in I_f and fibrosis of SAN.

DISCUSSION

The present study used a mouse model of hypertensive heart disease induced by sustained Ang II delivery to investigate the impacts of Ang II and hypertension on SAN function. Chronic Ang II treatment in mice is a well-established model of hypertension and cardiac hypertrophy (40). We showed that, in addition to producing these expected responses, chronic Ang II also results in overt SAN disease, as indicated by a reduction in HR (baseline and following autonomic blockade), a prolongation of cSNRT, and impaired conduction in the right atrial posterior wall in isolated atrial preparations. This is consistent with clinical data showing associations among hypertension, hypertrophy, and SAN disease (6). In addition, we studied the role of NPR-C in the progression of SAN disease. Strikingly, we found that Ang II treatment in NPR-$C^{-/-}$ mice greatly exacerbated disease progression. Specifically, NPR-$C^{-/-}$ mice treated with Ang II developed ventricular dilation with overt systolic heart failure (as opposed to compensated concentric hypertrophy in wild-type mice) and substantially more severe decline in SAN function. On the other hand, co-treatment of wild-type mice with Ang II and a selective NPR-C agonist (cANF) was able to largely prevent development of SAN disease. Several prior studies have demonstrated that cANF activates NPR-C without activating guanylyl cyclase-linked NPR-A and NPR-B (21,22,36). Furthermore, we previously showed that the acute effects of cANF in the heart are completely absent in NPR-$C^{-/-}$ mice (16,17), confirming the fact that cANF is a selective NPR-C agonist. Interestingly, our experiments suggest that Ang II treatment impaired SAN function in association with an inferior shift in the location of the leading pacemaker site (as assessed by optical mapping). This is consistent with studies in human and animal models of SAN disease that commonly show alterations in the location of the leading pacemaker site (6,25,41-43). Strikingly, co-treatment with cANF prevented this shift in leading activation site and resulted in SAN activations similar to that in saline-treated mice. Currently, there is a severe lack of therapeutic options for SAN disease. Our novel findings in mouse models suggest that NPR-C may be a viable new target for preventing the progression of SAN disease.

The responses observed in NPR-$C^{-/-}$ mice and in mice co-treated with cANF occurred without any differences in the hypertensive response to Ang II. NPR-$C^{-/-}$ mice treated with Ang II displayed the same degree of hypertension as wild-type mice, and cANF co-treatment did not prevent the increase in SBP elicited by Ang II. Some of the effects of Ang II on the hypertrophic response and cardiac remodeling are known to occur independently of blood pressure (44). Our findings suggest that this is also true in the context of SAN disease and indicate that NPR-C operates directly within the SAN, independently of SBP, to modulate the effects of Ang II. Interestingly, a previous study demonstrated that cANF could reduce blood pressure in spontaneously hypertensive rats, although the pressures observed in that model were substantially higher that those observed in our study of chronic Ang II treatment (23). If cANF can reduce blood pressure under some conditions, this may further contribute to the beneficial effects of NPR-C activation in hypertension. Collectively, our experiments indicate that cANF can modulate SAN function through direct effects in the SAN, independently of changes in SBP, supporting the idea that NPR-C is a viable target in the SAN in Ang II-mediated heart disease.

In previous studies (15,19) and the present one, we have shown that NPR-C is the most highly expressed NPR in the heart, including in the SAN. Our present study also demonstrates that chronic Ang II treatment does not alter the expression of NPR-C in the SAN, which is likely important in enabling NPR-C to be targeted with cANF. Nevertheless, there could be Ang II-induced changes in the expression of signaling molecules downstream of NPR-C, which could be affected differently in NPR-$C^{-/-}$ mice than in mice

co-treated with cANF. These will be useful areas for future investigation that will provide further insight into the mechanisms through which NPR-C and cANF affect Ang II-induced SAN dysfunction.

Our investigations of the mechanisms by which Ang II causes SAN disease revealed important roles for electrical remodeling in SAN myocytes (i.e., impaired spontaneous AP firing) as well as fibrosis of the SAN. In terms of electrical remodeling, our data illustrate that AP firing was impaired in association with reductions in the DD slope and I_f. Importantly, these Ang II-induced changes at the level of the SAN myocyte were indistinguishable between those in wild-type and NPR-C$^{-/-}$ mice. Rather, SAN disease was worse in NPR-C$^{-/-}$ mice due to a greater increase in SAN fibrosis in the absence of NPR-C. Interstitial fibrosis is a key component of SAN structure and a key determinant of SAN function, as studies have shown that the SAN contains higher levels of fibrosis than the working myocardium (10,12). Our data demonstrate levels of fibrosis in the SAN that are consistent with this. NPs are known to have potent antifibrotic effects in the heart, although most prior studies have focused on the roles of NPR-A and NPR-B in mediating these effects (45–49). Nevertheless, there is evidence that NPR-C can be involved in fibrotic signaling (50), and our previous work with NPR-C$^{-/-}$ mice shows that NPR-C regulates fibrosis by affecting collagen gene expression and collagen deposition in the heart, including in the SAN (19). The present study now demonstrates for the first time that loss of NPR-C greatly exacerbates the fibrotic response elicited by Ang II. Of particular importance is the novel finding that chronic, selective NPR-C activation potently prevents pathological collagen deposition in the SAN in Ang II-mediated heart disease. Collectively, these findings demonstrate a major role for NPR-C as a regulator of structural remodeling and fibrosis in the SAN and that this is a major determinant of the severity of SAN disease.

Studies of electrical remodeling at the level of the SAN myocyte (i.e., spontaneous AP morphology, ionic currents) in animal models of heart disease have been relatively scarce, and results have not always been consistent. For example, a study in a rabbit model of heart failure demonstrated SAN disease in association with a slowing of spontaneous AP firing, a reduction in DD slope and reduced I_f (1). Similarly, SAN disease has been described in canine studies of heart failure induced by atrial tachypacing (51,52). Although these studies did not directly measure SAN AP morphology, they did show that I_f density was reduced in association with reductions in expression of HCN2 and HNC4. Calcium currents were not altered in the SAN in any of those studies. On the other hand, a separate study using a chronic Ang II model reported that SAN disease occurred due to apoptosis of SAN myocytes (4). That study reported no differences in spontaneous AP firing or morphology in isolated SAN myocytes, and no ionic currents were investigated. Our experiments using a chronic Ang II model clearly demonstrate substantial changes in SAN AP firing patterns, as well as reductions in I_f. Consistent with the studies in rabbit and dog models of heart failure (1,51,52), we observed a reduction in expression of HCN4 in the SAN following Ang II treatment, which is consistent with the changes in AP cycle length, DD slope, and I_f density we observed. We also found no differences in $I_{Ca,L}$ in SAN myocytes following Ang II. Overall, our study supports the conclusion that spontaneous AP firing is compromised in hypertensive/Ang II-mediated heart disease and heart failure and that changes in expression of HCN channels and I_f density are a critical determinant of SAN disease. This is also consistent with data for other factors that contribute to SAN disease and dysfunction. For example, aging is a major contributor to SAN disease (5,25), and this has been shown to occur, at least in part, with a reduction in I_f (53). Similarly, endurance athletes exhibit bradycardia and a higher incidence of SAN disease in association with reductions in the expression of HCN4 and I_f density (54).

We also examined other potential mediators of electrical dysfunction by measuring the mRNA expression levels of *SCN5a*, *GJC1*, and *GJA1*. SCN5a has been shown to be present in the periphery of the SAN and to play a role in electrical conduction from the SAN to the atrial myocardium (32,55). We observed no changes in SCN5a expression in the SAN following Ang II treatment. Cx45 is a critical connexin in the SAN where it facilitates cell-to-cell communication (33); however, we observed no differences in Cx45 expression after Ang II treatment. Cx43 is primarily located in the atria and is mostly absent in the SAN, although strands of Cx43-positive tissue have been found to extend into the SAN (28,33,56). Furthermore, numerous studies have shown that Cx43 mRNA can be detected in the SAN (34,35,57). Accordingly, we measured Cx43 expression and found it was modestly reduced after Ang II treatment. Because the SAN is considered to be primarily a Cx43-negative region and the reduction we measured was very small, it is unlikely that a down-regulation of Cx43 contributed substantially to the

effects of Ang II on electrical conduction in the SAN. Nevertheless, we measured mRNA levels only for SCN5a, Cx45, and Cx43, and these targets could be altered in ways that do not involve changes in gene expression, which could be investigated in future studies.

In addition to preventing SAN fibrosis, we found that co-treatment with the NPR-C agonist cANF also dose-dependently prevented the reduction in I_f and changes in AP morphology induced by Ang II in SAN myocytes. As mentioned earlier, the reduction in I_f observed following Ang II treatment occurred in association with reduced HCN4 expression and no changes in I_f activation kinetics, indicating that reduced expression is the major determinant of the reduction in I_f. Similarly, the improved I_f densities observed following cANF co-treatment with Ang II occurred without changes in I_f activation kinetics. This suggests that cANF prevented the reduction in levels of HCN4 expression in the SAN observed in Ang II alone. Additional studies will be required to assess the effects of chronic cANF on ion channel expression in the SAN in Ang II-mediated heart disease, as well as the molecular mechanisms for any such effects. We have previously shown that acute application of NPs can modulate I_f in SAN myocytes isolated from normal wild-type mice and that these effects do involve changes in the voltage dependence of activation (15). Because we observed no such changes in our cANF co-treatment experiments, our data suggest that the chronic effects of cANF in heart disease are distinct from the acute effects of NPs in the normal SAN.

As mentioned, the impairments in electrical conduction in the SAN occurred in association with shifts in the location of the leading pacemaker site. The SAN is a heterogeneous structure (56), and it is conceivable that differences in expression levels of ion channels such as HCN4 in the superior and inferior pacemaker locations could contribute the alterations in function we observed. Furthermore, studies in the human and canine heart have demonstrated the existence of distinct SAN conduction pathways that can be accessed depending on location of leading pacemaker site (10,58,59), and this may further contribute to changes in SAN conduction. Although a study in human heart showed that HCN4 expression levels were similar in the head, the center, and the tail of the SAN (60), it is possible that there may be alterations in the diseased heart. Thus, it will be useful to explore the effects of Ang II on regional expression of HCN4 and possibly other channels (e.g., HCNs, calcium channels) in different parts of the SAN in future studies. It should be noted that our optical mapping studies did not resolve optical APs with double component upstrokes (i.e., an SAN component and an atrial component), which have been reported in other studies in large mammals and in mice (61–63). Identifying such APs would enable more specific assessments of SAN conduction velocities and thus could be pursued in future studies. We also note that the baseline beating rates in our isolated atrial preparations were lower than in ex vivo mouse hearts. This may be related to the effects of Di-4-ANNEPS, which can have some effects on sinus rate (64). Nevertheless, our isolated SAN myocyte and molecular studies, as well as histological assessments in the HCN-positive regions of the SAN, clearly support our conclusions from the effects of Ang II and NPR-C in the SAN.

STUDY LIMITATIONS. The present study focused on SAN dysfunction following Ang II treatment in mice. In addition, echocardiographic data demonstrated that Ang II treatment caused concentric ventricular hypertrophy in wild-type mice and ventricular dilation and heart failure in NPR-$C^{-/-}$ mice. These findings suggest that NPR-C might have affected electrical or structural remodeling in the ventricles as well. Similarly, Ang II treatment has been shown to cause atrial fibrillation (65,66), and it is possible that NPR-C affects atrial remodeling in addition to its effects in the SAN. Although our study demonstrates important effects of NPR-C in the SAN, it is also important to recognize that global ablation of NPR-C and systemic application of cANF can also have noncardiac effects. Although these were not the foci of our study, it is conceivable that treatment with NPs could have effects on the vasculature, kidneys, and other systems that may further affect disease progression. These areas will be important for additional studies. Our study was conducted in mouse models, which was essential for identifying new roles for NPR-C using knockout mice. It will be important to validate these findings in large animal models and ultimately in human patients.

Efforts to develop new therapeutic approaches for SAN disease are focused on the development of new pharmacological agents as well as the possibility of using biological pacemakers (67,68). Interestingly, several studies in the area of biological pacemakers have focused on strategies that upregulate HCN channel expression, either directly or through specific transcription factors such as Tbx18 (69–71). Our results illustrate that targeting NPR-C offers another approach to modulating HCN expression and I_f density in SAN disease. There is

great interest in the design and use of synthetic NPs for the treatment of heart disease (72–75). Our findings indicate that compounds targeting NPR-C should be considered in the design of new agents and that these could be useful in the context of SAN disease.

CONCLUSIONS

Data demonstrate that SAN disease in the setting of hypertension and elevated Ang II involves both electrical remodeling (i.e., changes in ion channel function in SAN myocytes) and structural remodeling (i.e., fibrosis) in mice. Our studies identified the novel approach of targeting NPR-C to prevent both electrical and structural remodeling in the SAN during chronic Ang II treatment, which had highly beneficial effects on SAN function in vivo. The observation that both of these processes are preventable by activation of NPR-C helps explain the potent beneficial effects of targeting this NP receptor and demonstrates that synthetic NPs that activate NPR-C could offer a 2-pronged approach to prevent major cellular and molecular determinants of the progression of SAN disease in the setting of Ang II-mediated hypertension, hypertrophy, and heart failure.

ADDRESS FOR CORRESPONDENCE: Prof. Robert Alan Rose, Libin Cardiovascular Institute of Alberta, Cumming School of Medicine, University of Calgary, GAC66, Health Research Innovation Centre, 3280 Hospital Drive NW, Calgary, Alberta, Canada T2N 4Z6. E-mail: robert.rose@ucalgary.ca.

PERSPECTIVES

COMPETENCY IN MEDICAL KNOWLEDGE: SAN disease is prevalent in hypertension and heart failure, conditions characterized by elevated Ang II signaling. The mechanisms responsible for SAN disease remain poorly understood, which limits therapeutic options.

TRANSLATIONAL OUTLOOK: Our studies provide new insight into the mechanistic basis for Ang II- induced SAN disease in mice. We show that Ang II impairs spontaneous SAN myocyte action potential firing by decreasing the slope of the diastolic depolarization and reducing the hyperpolarization-activated current (I_f). Ang II also causes SAN fibrosis. Our study shows that NPR-C may represent a new target to prevent these impairments in SAN function. Additional studies are required to determine how to translate these findings to human patients.

REFERENCES

1. Verkerk AO, Wilders R, Coronel R, et al. Ionic remodeling of sinoatrial node cells by heart failure. Circulation 2003;108:760–6.

2. Sanders P, Kistler PM, Morton JB, et al. Remodeling of sinus node function in patients with congestive heart failure: reduction in sinus node reserve. Circulation 2004;110:897–903.

3. Janse MJ. Electrophysiological changes in heart failure and their relationship to arrhythmogenesis. Cardiovasc Res 2004;61:208–17.

4. Swaminathan PD, Purohit A, Soni S, et al. Oxidized CaMKII causes cardiac sinus node dysfunction in mice. J Clin Invest 2011;121:3277–88.

5. Dobrzynski H, Boyett MR, Anderson RH. New insights into pacemaker activity: promoting understanding of sick sinus syndrome. Circulation 2007;115:1921–32.

6. Morris GM, Kalman JM. Fibrosis, electrics and genetics. Perspectives in sinoatrial node disease. Circ J 2014;78:1272–82.

7. Swaminathan PD, Purohit A, Hund TJ, et al. Calmodulin-dependent protein kinase II: linking heart failure and arrhythmias. Circ Res 2012;110:1661–77.

8. Fedorov VV, Glukhov AV, Chang R. Conduction barriers and pathways of the sinoatrial pacemaker complex: their role in normal rhythm and atrial arrhythmias. Am J Physiol Heart Circ Physiol 2012;302:H1773–83.

9. Mangoni ME, Nargeot J. Genesis and regulation of the heart automaticity. Physiol Rev 2008;88:919–82.

10. Li N, Hansen BJ, Csepe TA, et al. Redundant and diverse intranodal pacemakers and conduction pathways protect the human sinoatrial node from failure. Sci Transl Med 2017 Jul 26;9(400). pii: eaam5607.

11. Lakatta EG, Maltsev VA, Vinogradova TM. A coupled SYSTEM of intracellular Ca2+ clocks and surface membrane voltage clocks controls the timekeeping mechanism of the heart's pacemaker. Circ Res 2010;106:659–73.

12. Csepe TA, Kalyanasundaram A, Hansen BJ, et al. Fibrosis: a structural modulator of sinoatrial node physiology and dysfunction. Front Physiol 2015;6:37.

13. Rose RA, Giles WR. Natriuretic peptide C receptor signalling in the heart and vasculature. J Physiol 2008;586:353–66.

14. Moghtadaei M, Polina I, Rose RA. Electrophysiological effects of natriuretic peptides in the heart are mediated by multiple receptor subtypes. Prog Biophys Mol Biol 2016;120:37–49.

15. Springer J, Azer J, Hua R, et al. The natriuretic peptides BNP and CNP increase heart rate and electrical conduction by stimulating ionic currents in the sinoatrial node and atrial myocardium following activation of guanylyl cyclase-linked natriuretic peptide receptors. J Mol Cell Cardiol 2012;52:1122–34.

16. Azer J, Hua R, Vella K, et al. Natriuretic peptides regulate heart rate and sinoatrial node function by activating multiple natriuretic peptide receptors. J Mol Cell Cardiol 2012;53:715–24.

17. Azer J, Hua R, Krishnaswamy PS, et al. Effects of natriuretic peptides on electrical conduction in the sinoatrial node and atrial myocardium of the heart. J Physiol 2014;592:1025–45.

18. Rose RA, Lomax AE, Kondo CS, et al. Effects of C-type natriuretic peptide on ionic currents in mouse sinoatrial node: a role for the NPR-C receptor. Am J Physiol Heart Circ Physiol 2004;286:H1970–7.

19. Egom EE, Vella K, Hua R, et al. Impaired sinoatrial node function and increased susceptibility to atrial fibrillation in mice lacking natriuretic peptide receptor C. J Physiol 2015;593:1127–46.

20. Hua R, MacLeod SL, Polina I, et al. Effects of wild-type and mutant forms of atrial natriuretic peptide on atrial electrophysiology and arrhythmogenesis. Circ Arrhythm Electrophysiol 2015;8:1240–54.

21. Anand-Srivastava MB, Sairam MR, Cantin M. Ring-deleted analogs of atrial natriuretic factor inhibit adenylate cyclase/cAMP system. Possible coupling of clearance atrial natriuretic factor receptors to adenylate cyclase/cAMP signal transduction system. J Biol Chem 1990;265:8566–72.

22. Anand-Srivastava MB, Sehl PD, Lowe DG. Cytoplasmic domain of natriuretic peptide receptor-C inhibits adenylyl cyclase. Involvement of a pertussis toxin-sensitive G protein. J Biol Chem 1996;271:19324–9.

23. Li Y, Sarkar O, Brochu M, et al. Natriuretic peptide receptor-C attenuates hypertension in spontaneously hypertensive rats: role of nitro-oxidative stress and gi proteins. Hypertension 2014; 63:846–55.

24. Krishnaswamy PS, Egom EE, Moghtadaei M, et al. Altered parasympathetic nervous system regulation of the sinoatrial node in Akita diabetic mice. J Mol Cell Cardiol 2015;82:125–35.

25. Moghtadaei M, Jansen HJ, Mackasey M, et al. The impacts of age and frailty on heart rate and sinoatrial node function. J Physiol 2016;594: 7105–26.

26. Fedorov VV, Lozinsky IT, Sosunov EA, et al. Application of blebbistatin as an excitation-contraction uncoupler for electrophysiologic study of rat and rabbit hearts. Heart Rhythm 2007;4:619–26.

27. El Khoury N, Mathieu S, Marger L, et al. Upregulation of the hyperpolarization-activated current increases pacemaker activity of the sino-atrial node and heart rate during pregnancy in mice. Circulation 2013;127:2009–20.

28. Liu J, Dobrzynski H, Yanni J, et al. Organisation of the mouse sinoatrial node: structure and expression of HCN channels. Cardiovasc Res 2007; 73:729–38.

29. Cifelli C, Rose RA, Zhang H, et al. RGS4 regulates parasympathetic signaling and heart rate control in the sinoatrial node. Circ Res 2008;103: 527–35.

30. Zhang Z, Xu Y, Song H, et al. Functional Roles of Ca(v)1.3 (alpha(1D)) calcium channel in sinoatrial nodes: insight gained using gene-targeted null mutant mice. Circ Res 2002;90:981–7.

31. Mangoni ME, Couette B, Bourinet E, et al. Functional role of L-type Cav1.3 Ca2+ channels in cardiac pacemaker activity. Proc Natl Acad Sci U S A 2003;100:5543–8.

32. Lei M, Zhang H, Grace AA, et al. SCN5A and sinoatrial node pacemaker function. Cardiovasc Res 2007;74:356–65.

33. Verheijck EE, van Kempen MJ, Veereschild M, et al. Electrophysiological features of the mouse sinoatrial node in relation to connexin distribution. Cardiovasc Res 2001;52:40–50.

34. Tellez JO, Dobrzynski H, Greener ID, et al. Differential expression of ion channel transcripts in atrial muscle and sinoatrial node in rabbit. Circ Res 2006;99:1384–93.

35. Marionneau C, Couette B, Liu J, et al. Specific pattern of ionic channel gene expression associated with pacemaker activity in the mouse heart. J Physiol 2005;562:223–34.

36. Pagano M, Anand-Srivastava MB. Cytoplasmic domain of natriuretic peptide receptor C constitutes Gi activator sequences that inhibit adenylyl cyclase activity. J Biol Chem 2001;276:22064–70.

37. Izumiya Y, Araki S, Usuku H, et al. Chronic C-type natriuretic peptide infusion attenuates angiotensin II-induced myocardial superoxide production and cardiac remodeling. Int J Vasc Med 2012;2012:246058.

38. O'Connor CM, Starling RC, Hernandez AF, et al. Effect of nesiritide in patients with acute decompensated heart failure. N Engl J Med 2011; 365:32–43.

39. Thireau J, Karam S, Fauconnier J, et al. Functional evidence for an active role of B-type natriuretic peptide in cardiac remodelling and pro-arrhythmogenicity. Cardiovasc Res 2012;95: 59–68.

40. Houser SR, Margulies KB, Murphy AM, et al. Animal models of heart failure: a scientific statement from the American Heart Association. Circ Res 2012;111:131–50.

41. Glukhov AV, Kalyanasundaram A, Lou Q, et al. Calsequestrin 2 deletion causes sinoatrial node dysfunction and atrial arrhythmias associated with altered sarcoplasmic reticulum calcium cycling and degenerative fibrosis within the mouse atrial pacemaker complex1. Eur Heart J 2015;36: 686–97.

42. John RM, Kumar S. Sinus node and atrial arrhythmias. Circulation 2016;133:1892–900.

43. Joung B, Hwang HJ, Pak HN, et al. Abnormal response of superior sinoatrial node to sympathetic stimulation is a characteristic finding in patients with atrial fibrillation and symptomatic bradycardia. Circ Arrhythm Electrophysiol 2011;4: 799–807.

44. Kim S, Iwao H. Molecular and cellular mechanisms of angiotensin II-mediated cardiovascular and renal diseases. Pharmacol Rev 2000;52:11–34.

45. Calvieri C, Rubattu S, Volpe M. Molecular mechanisms underlying cardiac antihypertrophic and antifibrotic effects of natriuretic peptides. J Mol Med (Berl) 2012;90:5–13.

46. Tsuruda T, Boerrigter G, Huntley BK, et al. Brain natriuretic peptide is produced in cardiac fibroblasts and induces matrix metalloproteinases. Circ Res 2002;91:1127–34.

47. Horio T, Tokudome T, Maki T, et al. Gene expression, secretion, and autocrine action of C-type natriuretic peptide in cultured adult rat cardiac fibroblasts. Endocrinology 2003;144: 2279–84.

48. Kapoun AM, Liang F, O'Young G, et al. B-type natriuretic peptide exerts broad functional opposition to transforming growth factor-beta in primary human cardiac fibroblasts: fibrosis, myofibroblast conversion, proliferation, and inflammation. Circ Res 2004;94:453–61.

49. Jansen HJ, Rose RA. Natriuretic peptides: critical regulators of cardiac fibroblasts and the extracellular matrix in the heart. In: Dixon IM, Wigle JT, editors. Cardiac Fibrosis and Heart Failure: Cause or Effect. Springer International Publishing, 2015:383–404.

50. Huntley BK, Sandberg SM, Noser JA, et al. BNP-induced activation of cGMP in human cardiac fibroblasts: interactions with fibronectin and natriuretic peptide receptors. J Cell Physiol 2006; 209:943–9.

51. Yeh YH, Burstein B, Qi XY, et al. Funny current downregulation and sinus node dysfunction associated with atrial tachyarrhythmia: a molecular basis for tachycardia-bradycardia syndrome. Circulation 2009;119:1576–85.

52. Zicha S, Fernandez-Velasco M, Lonardo G, et al. Sinus node dysfunction and hyperpolarization-activated (HCN) channel subunit remodeling in a canine heart failure model. Cardiovasc Res 2005;66:472–81.

53. Larson ED, St Clair JR, Sumner WA, et al. Depressed pacemaker activity of sinoatrial node myocytes contributes to the age-dependent decline in maximum heart rate. Proc Natl Acad Sci U S A 2013;110:18011–6.

54. D'Souza A, Bucchi A, Johnsen AB, et al. Exercise training reduces resting heart rate via downregulation of the funny channel HCN4. Nat Commun 2014;5:3775.

55. Lei M, Goddard C, Liu J, et al. Sinus node dysfunction following targeted disruption of the murine cardiac sodium channel gene Scn5a. J Physiol 2005;567:387–400.

56. Boyett MR, Honjo H, Kodama I. The sinoatrial node, a heterogeneous pacemaker structure. Cardiovasc Res 2000;47:658–87.

57. Tellez JO, McZewski M, Yanni J, et al. Ageing-dependent remodelling of ion channel and Ca2+ clock genes underlying sino-atrial node pacemaking. Exp Physiol 2011;96:1163–78.

58. Fedorov VV, Glukhov AV, Chang R, et al. Optical mapping of the isolated coronary-perfused human sinus node. J Am Coll Cardiol 2010;56: 1386–94.

59. Fedorov VV, Schuessler RB, Hemphill M, et al. Structural and functional evidence for discrete exit pathways that connect the canine sinoatrial node and atria. Circ Res 2009;104:915–23.

60. Li N, Csepe TA, Hansen BJ, et al. Molecular mapping of sinoatrial node HCN channel expression in the human heart. Circ Arrhythm Electrophysiol 2015;8:1219–27.

61. Fedorov VV, Chang R, Glukhov AV, et al. Complex interactions between the sinoatrial node and atrium during reentrant arrhythmias in the canine heart. Circulation 2010;122:782–9.

62. Lang D, Glukhov AV. High-resolution optical mapping of the mouse sino-atrial node. J Vis Exp 2016 Dec 2;(118). https://doi.org/10.3791/54773.

63. Efimov IR, Fedorov VV, Joung B, et al. Mapping cardiac pacemaker circuits: methodological puzzles of the sinoatrial node optical mapping. Circ Res 2010;106:255–71.

64. Matiukas A, Mitrea BG, Qin M, et al. Near-infrared voltage-sensitive fluorescent dyes optimized for optical mapping in blood-perfused myocardium. Heart Rhythm 2007;4:1441–51.

65. Purohit A, Rokita AG, Guan X, et al. Oxidized Ca2+/calmodulin-dependent protein kinase II triggers atrial fibrillation. Circulation 2013;128: 1748–57.

66. Li J, Wang S, Bai J, et al. Novel Role for the immunoproteasome subunit PSMB10 in angiotensin II-induced atrial fibrillation in mice. Hypertension 2018;71:866–76.

67. Siu CW, Lieu DK, Li RA. HCN-encoded pacemaker channels: from physiology and biophysics to bioengineering. J Membr Biol 2006;214:115–22.

68. Cho HC. Pacing the heart with genes: recent progress in biological pacing. Curr Cardiol Rep 2015;17:65.

69. Sun Y, Timofeyev V, Dennis A, et al. A singular role of IK1 promoting the development of cardiac automaticity during cardiomyocyte differentiation by IK1-induced activation of pacemaker current. Stem Cell Rev 2017;13:631–43.

70. Tse HF, Xue T, Lau CP, et al. Bioartificial sinus node constructed via in vivo gene transfer of an engineered pacemaker HCN channel reduces the dependence on electronic pacemaker in a sick-sinus syndrome model. Circulation 2006;114:1000–11.

71. Kapoor N, Liang W, Marban E, et al. Direct conversion of quiescent cardiomyocytes to pacemaker cells by expression of Tbx18. Nat Biotechnol 2013;31:54–62.

72. Cataliotti A, Burnett JC Jr. Natriuretic peptides: novel therapeutic targets in heart failure. J Investig Med 2005;53:378–84.

73. Lee CY, Lieu H, Burnett JC Jr. Designer natriuretic peptides. J Investig Med 2009;57:18–21.

74. Rose RA. CD-NP, a chimeric natriuretic peptide for the treatment of heart failure. Curr Opin Investig Drugs 2010;11:349–56.

75. Volpe M, Rubattu S, Burnett J Jr. Natriuretic peptides in cardiovascular diseases: current use and perspectives. Eur Heart J 2014;35:419–25.

KEY WORDS fibrosis, hypertension, ion currents, natriuretic peptide, sinoatrial node

APPENDIX For an expanded Methods section, please see the online version of this paper.

Supplemental Information

Natriuretic peptide receptor C (NPR-C) protects against angiotensin II mediated sinoatrial node disease in mice

Methods

Mice

Littermate male wildtype and NPR-C$^{-/-}$ mice were initially obtained from the Jackson Laboratory (strain B6;C-*Npr3lgj*/J) and backcrossed into the C57Bl/6 line as we have previously reported (1-3).

In vivo electrophysiology

HR was measured in anesthetized mice (2% isoflurane) using 30 gauge subdermal needle electrodes (Grass Technologies) to record body surface (lead II) ECGs. In parallel, a 1.2 French octapolar electrophysiology catheter was inserted in the right heart via the jugular vein and used for intracardiac programmed stimulation experiments, as we have described previously (2,4). Correct catheter placement was ensured by obtaining a sole ventricular signal in the distal lead and a predominant atrial signal in the proximal lead. All stimulation pulses were given at 3 V for 2 ms, which enabled continuous capture and drive of cardiac conduction. Sinoatrial node recovery time (SNRT) was measured by delivering a 12 stimulus drive train at a cycle length of 100 ms. SNRT is defined as the time between the last stimulus in the drive train and the occurrence of the first spontaneous atrial beat (P wave). SNRT was corrected for heart rate (cSNRT) by subtracting the prestimulus RR interval from the measured SNRT. Data were acquired using a Gould ACQ-7700 amplifier and Ponemah Physiology Platform software (Data Sciences International). Body temperature was monitored continuously via a rectal probe and maintained at 37°C with a heating pad.

High resolution optical mapping

To investigate patterns of electrical conduction in the SAN we used high resolution optical mapping in atrial preparations as we have described previously (2,4,5). Hearts were excised into Krebs solution (35°C) containing (in mM): 118 NaCl, 4.7 KCl, 1.2 KH_2PO_4, 12.2 $MgSO_4$, 1 $CaCl_2$, 25 $NaHCO_3$, 11 glucose and bubbled with 95% O_2/5% CO_2 in order to maintain a pH of 7.4. The atrial preparation was superfused continuously with Krebs solution (37°C) bubbled with 95% O_2/5% CO_2 and allowed to equilibrate for at least 30 min. During this time the preparation was treated with the voltage sensitive dye di-4-ANEPPS (10 μM) and blebbistatin (10 μM) was added to the superfusate to suppress contractile activity. Blebbistatin was present throughout the duration of the experiments in order prevent motion artifacts during optical mapping (6). Experiments were performed in sinus rhythm so that the cycle length (i.e. beating rate) of the atrial preparation was free to change.

Di-4-ANEPPS loaded atrial preparations were illuminated with light at a wavelength of 520 – 570 nM using an EXFO X-cite fluorescent light source (Lumen Dynamics). Emitted fluorescent light (590 – 640 nm) was captured using a high speed EMCCD camera (Evolve 128, Photometrics). We mapped conduction in the region of the right atrial posterior wall around the point of initial electrical excitation, which corresponds to the activation of the SAN (2,4,7). The region that was mapped extended from the superior vena cava to the inferior cava along the edge of the crista terminalis, based on the known anatomical location of the SAN in the mouse heart (8). In these studies, the spatial resolution of each pixel was 45 x 45 μM and data were acquired at ~900 frames/s using Metamorph software (Molecular Devices). Magnification was constant in all experiments and no pixel binning was used.

All optical data were analyzed using custom software written in Matlab (version 9.1). Analyses included pseudocolor electrical activation maps, which were generated from measurements of activation time at individual pixels. In each case background fluorescence was subtracted. Local conduction velocity (CV) was quantified in the right atrial posterior wall

around the site of initial electrical activation using an approach previously described by us and others (4,5,9,10). Briefly, activation times at each pixel from a 7 x 7 pixel array were determined and fit to a plane using the least squares fit method. The direction on this plane that is increasing the fastest represents the direction that is perpendicular to the wavefront of electrical propagation and the maximum slope represents the inverse of the speed of conduction in that direction. Using this method, we computed maximum local CV vectors in the SAN around the leading pacemaker site. With pixel dimensions of 50 x 50 μM, the area of the 7 x 7 pixel array was 350 x 350 μM, which is within the anatomical area of the mouse SAN (8). Optical action potentials were measured by assessing changes in fluorescence as a function of time at individual pixels within the SAN as we have described previously (4,5).

Patch-clamping of isolated SAN myocytes

The procedures for isolating single pacemaker myocytes from the sinoatrial node (SAN), of the mouse have been described previously (1,2) and were as follows. Mice were administered a 0.2 ml intraperitoneal injection of heparin (1000 IU/ml) to prevent blood clotting. Following this, mice were anesthetized by isoflurane inhalation and then euthanized by cervical dislocation. The heart was excised into Tyrode's solution (35ºC) consisting of (in mmol/L) 140 NaCl, 5.4 KCl, 1.2 KH_2PO_4, 1.0 $MgCl_2$, 1.8 $CaCl_2$, 5.55 glucose, and 5 HEPES, with pH adjusted to 7.4 with NaOH. The sinoatrial node (SAN) region of the heart was isolated by separating the atria from the ventricles, cutting open the superior and inferior venae cavae, and pinning the tissue so that the crista terminalis could be identified. The SAN area is located in the intercaval region adjacent to the crista terminalis. This SAN region was cut into strips, which were transferred and rinsed in a 'low Ca^{2+}, Mg^{2+} free' solution containing (in mmol/L) 140 NaCl, 5.4 KCl, 1.2 KH_2PO_4, 0.2 $CaCl_2$, 50 taurine, 18.5 glucose, 5 HEPES and 1 mg/ml bovine serum albumin (BSA), with pH adjusted to 6.9 with NaOH. SAN tissue strips were digested in 5 ml of 'low Ca^{2+}, Mg^{2+} free' solution containing collagenase (type II, Worthington Biochemical

Corporation), elastase (Worthington Biochemical Corporation) and protease (type XIV, Sigma Chemical Company) for 30 min. Then the tissue was transferred to 5 ml of modified KB solution containing (in mmol/L) 100 potassium glutamate, 10 potassium aspartate, 25 KCl, 10 KH_2PO_4, 2 $MgSO_4$, 20 taurine, 5 creatine, 0.5 EGTA, 20 glucose, 5 HEPES, and 0.1% BSA, with pH adjusted to 7.2 with KOH. The tissue was mechanically agitated using a wide-bore pipette. This procedure yielded individual SAN myocytes with cellular automaticity that was recovered after readapting the cells to a physiological concentration of Ca^{2+}. SAN myocytes were identified by their small spindle shape and ability to beat spontaneously in the recording chamber when superfused with normal Tyrode's solution. When patch-clamped, SAN myocytes displayed spontaneous action potentials and the hyperpolarization-activated current, I_f. The capacitance of single SAN myocytes was 20 – 35 pF.

Spontaneous action potentials (APs) and stimulated APs were recorded using the perforated patch-clamp technique on single SAN. The hyperpolarization-activated current (I_f) and L-type Ca^{2+} currents ($I_{Ca,L}$) were recorded by voltage clamping single SAN using the patch-clamp technique in the whole cell configuration. APs and membrane currents were recorded at room temperature (22-23℃), which must be noted when comparing AP frequency in isolated cells to beating rates *in vivo* or in isolated hearts at body temperature.

For recording APs and I_f the recording chamber was superfused with a normal Tyrode's solution (22 – 23ºC) containing (in mmol/L) 140 NaCl, 5 KCl, 1 $MgCl_2$, 1 $CaCl_2$, 10 HEPES, and 5 glucose, with pH adjusted to 7.4 with NaOH. The pipette filling solution for I_f contained (in mmol/L) 135 KCl, 0.1 $CaCl_2$, 1 $MgCl_2$, 5 NaCl, 10 EGTA, 4 Mg-ATP, 6.6 Na-phosphocreatine, 0.3 Na-GTP and 10 HEPES, with pH adjusted to 7.2 with KOH. Amphotericin B (200 µg/ml) was added to this pipette solution to record APs or I_f with the perforated patch clamp technique. $BaCl_2$ (1×10^{-4} mol/L) was added to the superfusate when recording I_f, in order to eliminate any inward rectifier K^+ current that could be present at low levels in some SAN myocytes.

For recording $I_{Ca,L}$ SAN myocytes were superfused with a modified Tyrode's solution (22 – 23 ℃) containing the following (in mmol/L) 140 TEA-Cl, 5.4 CsCl, 2 $CaCl_2$, 1 $MgCl_2$, 10 HEPES, and 5 glucose with pH adjusted to 7.4 with CsOH. The pipette solution for $I_{Ca,L}$ contained (in mmol/L) 135 CsCl, 0.2 $CaCl_2$, 1 $MgCl_2$, 5 NaCl, 5 EGTA, 4 Mg-ATP, 6.6 Na-phosphocreatine, 0.3 Na-GTP and 10 HEPES, with pH adjusted to 7.2 with CsOH. This approach was used in order to record $I_{Ca,L}$ from a holding potential of -60 mV due to the expression of $Ca_V1.2$ and $Ca_V1.3$ in SAN cells (11,12).

Micropipettes were pulled from borosilicate glass (with filament, 1.5 mm OD, 0.75 mm ID, Sutter Instrument Company) using a Flaming/Brown pipette puller (model p-87, Sutter Instrument Company). The resistance of these pipettes was 4 – 8 MΩ when filled with recording solution. Micropipettes were positioned with a micromanipulator (Burleigh PCS-5000 system) mounted on the stage of an inverted microscope (Olympus IX71). Seal resistance was 2 – 15 GΩ. Rupturing the sarcolemma in the patch for voltage clamp experiments resulted in access resistances of 5 – 15 MΩ. Series resistance compensation averaged 80 – 85% using an Axopatch 200B amplifier (Molecular Devices). For perforated patch clamp experiments access resistance was monitored for the development of capacitative transients upon sealing to the cell membrane with Amphotericin B in the pipette. Typically, access resistance became less than 30 MΩ within 5 min of sealing onto the cell, which was sufficient for recording spontaneous APs in current clamp mode. Data were digitized using a Digidata 1440 and pCLAMP 10 software (Molecular Devices) and stored on computer for *post hoc* analysis.

Spontaneous AP parameters, including the maximum diastolic potential (MDP), the slope of the diastolic depolarization (DD slope), the maximum AP upstroke velocity (Vmax), the AP overshoot and the AP duration at 50% repolarization (APD_{50}) were analyzed. The DD slope was measured by fitting a straight line to the linear portion of this AP component.

Activation kinetics for I_f were determined by normalizing tail currents at each voltage to the maximum current level at -130 mV and fitting the data to the Boltzmann function:

$I/I_{max}=1/(1+\exp[(V_m-V_{1/2})/k])$ where V_m is the potential of the voltage clamp step, $V_{1/2}$ is the voltage at which 50% activation occurs and k is the slope factor. $I_{Ca,L}$ activation kinetics were determined by calculating chord conductance (G) with the equation $G=I/(V_m-E_{rev})$, where V_m represents the depolarizing voltages and E_{rev} is the reversal potential estimated from the current-voltage relation of $I_{Ca,L}$. Maximum conductance (G_{max}) and $V_{1/2}$ of activation for $I_{Ca,L}$ were determined using the following function: $G=[(V_m-V_{rev})][G_{max}][-1/[(1+\exp((V_m-V_{1/2})/k))+1]]$.

Quantitative PCR

Quantitative gene expression in the SAN was performed as we described previously (1,4). Intron spanning primers (Integrated DNA Technologies) were designed for NPR-A, NPR-B, NPR-C, HCN1, HCN2, HCN4, SCN5a, Cx43 and Cx45. GAPDH was used as the reference gene. Primer sequences are provided in Table S5. Following synthesis primers were reconstituted in nuclease free water at a concentration of 100 μM and stored at -20°C. All primer sets were validated in order to determine optimal annealing temperature as well as confirmation of ideal amplification efficiency (between 90-110% copy efficiency per cycle).

RNA was extracted in PureZOL™ RNA isolation reagent according to kit instructions (Aurum Total RNA Fatty and Fibrous Tissue Kit, Bio-Rad). RNA was eluted in 40 μl of elution buffer from the spin column. RNA concentrations were determined using a Qubit fluorometer (Invitrogen) and first strand synthesis reactions were performed using the iScript cDNA synthesis kit (Bio-Rad) according to kit instructions. The Experion™ Automated Electrophoresis System (Bio-Rad) was used to assess RNA quality by observing the 28S and 18S rRNA subunits prior to first strand synthesis. Lack of genomic DNA contamination was verified by reverse transcription (RT)-PCR using a no RT control.

RT-qPCR using BRYT green dye (Promega) was used to assess gene expression. Following RNA extraction, cDNA was synthesized and 10μl reactions were performed with 5.6μl of SYBR green dye, 4μl cDNA template (at the appropriate dilution), and 0.4μl of primers.

Primers were used at a concentration of 10 nM except HCN2, which was used at 500 nM. Reactions were carried out using the CFX384 Touch™ Real-Time PCR Detection System (Bio-Rad). Amplification conditions were as follows: 95°C for 2 minutes to activate Taq polymerase, followed by 39 cycles of denaturation at 95°C for 15 seconds, annealing at 60°C for 30 seconds, and extension at 72°C for 30 seconds. Melt curve analysis was performed from 65-95°C in 0.5°C increments. Single amplicons with appropriate melting temperatures and sizes were detected. Data were analyzed and expression values were normalized to GAPDH.

Western blotting

Protein samples were extracted from two SANs and pooled for each experimental replicate in order to ensure sufficient protein (13). In other studies, singe right and left atria were used for protein extractions. Tissues were pre-cooled in liquid nitrogen and homogenized in an ice-cold RIPA buffer (50mM Tris, 150mM NaCl, 1mM EDTA, 25mM sucrose, 1% Triton, 0.1% SDS) containing 0.5mM DTT (1,4-Dithiothreitol, Roche) and Protease Inhibitor Cocktail (Sigma-Aldrich). Preparation was centrifuged at 10000rpm at 4^0C for 10mins. Protein concentrations were measured using a Bio-Rad *DC*™ Protein Assay Kit II (Bio-Rad). Protein samples (20 µg/lane) were separated by 12 % SDS-polyacrylamide gels (SDS-PAGE) and transferred onto Biotrace™ NT nitrocellulose Transfer Membrane (VWR). The membrane was blocked with 1% casein in tris-buffered saline (TBS; Bio-Rad) for 1 hour and incubated overnight at 4^0C with rabbit primary antibodies (NPR-A 1:200, NPR-B 1:1000, NPR-C 1:200, HCN4 1:200 and GAPDH 1:5000, Abcam). The membrane was washed 3 times with TBST (TBS with 1% Tween 20 (Bio-Rad)) and incubated with goat anti-rabbit IgG coupled to horseradish peroxidase (HRP; Abcam) at 1:20000 for 1 hour at room temperature. Then the membrane was washed again 3 times with TBST. ECL (Bio-Rad) was added, incubated for 5 min and the membrane was scanned using the ChemiDoc system (Bio-Rad). After NPR-B detection, the membrane was stripped using mild stripping buffer (0.15% glycine, 0.1% SDS and 1% tween20), washed with

PBST and incubated for NPR-A detection. The HCN4 antibody was obtained from Alomone Labs while the NPR-A, NPR-B, NPR-C and GAPDH antibodies were obtained from Abcam. We quantified expression of each of these proteins based on the identification of bands at the predicted molecular according to the information from the supplier.

Histology and immunohistochemistry

Interstitial fibrosis was assessed using picrosirius red (collagen) and fast green (myocardium) staining of paraffin embedded sections (8 µM) through the SAN cut perpendicular to the crista terminalis. Adjacent sections were used for immunostaining of HCN4 in order to confirm the SAN region as we (14) and others (8) have described previously. For the immunohistochemistry, sections were deparaffinised and blocked for 1 hr with 15% goat serum (Gibco). Sections were then incubated with anti-HCN4 primary antibody (Alomone Labs) at a dilution of 1:100 overnight in a light –protected chamber. Sections were then incubated with Alexa Fluor 488 Goat anti-Rabbit IgG (H+L; Invitrogen) secondary antibody at a dilution of 1:100 for 1 hr at room temperature. Sections were mounted with ProLong Gold Antifade Mountant (Invitrogen) and imaged by confocal microscopy at 488/519 nm (Zeiss LSM 5 Exciter).

Supplemental Figures

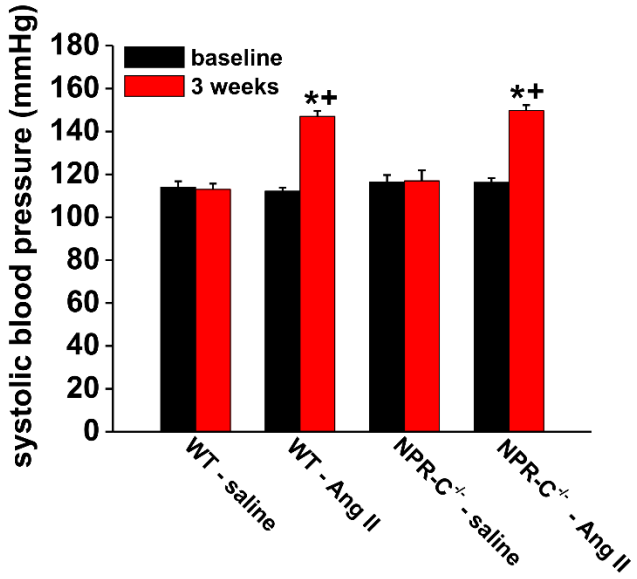

Supplemental Figure 1. Systolic blood pressure measurements in wildtype and NPR-C$^{-/-}$ mice treated with Ang II. Measurements were taken at baseline and following 3 weeks of saline or Ang II treatment. *P<0.001 vs. baseline within treatment group, ^{+}P<0.001 vs saline at 3 week time point, P=0.115 between genotypes within treatment group by two-way ANOVA with Tukey's post-hoc test, n=17 mice for wildtype/saline, 18 mice for wildtype/Ang II, 11 mice for NPR-C$^{-/-}$/saline and 11 mice for NPR-C$^{-/-}$/Ang II.

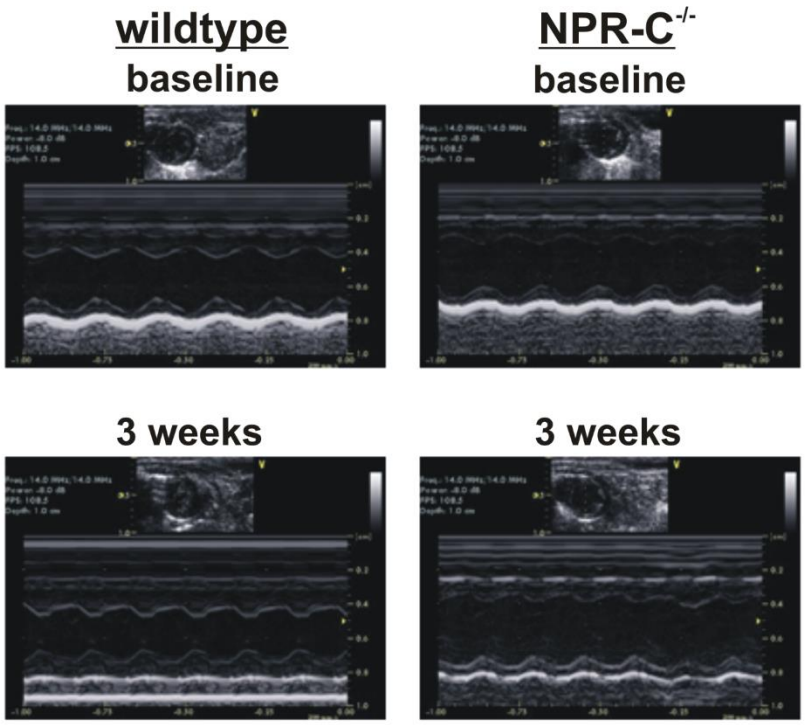

Supplemental Figure 2. Echocardiography on wildtype and NPR-C$^{-/-}$ mice treated with Ang II. M-mode imaging of the left ventricle from the parasternal short axis view at the midpapillary level at baseline and following 3 weeks of Ang II treatment. Refer to Supplemental Table 1 for summary data.

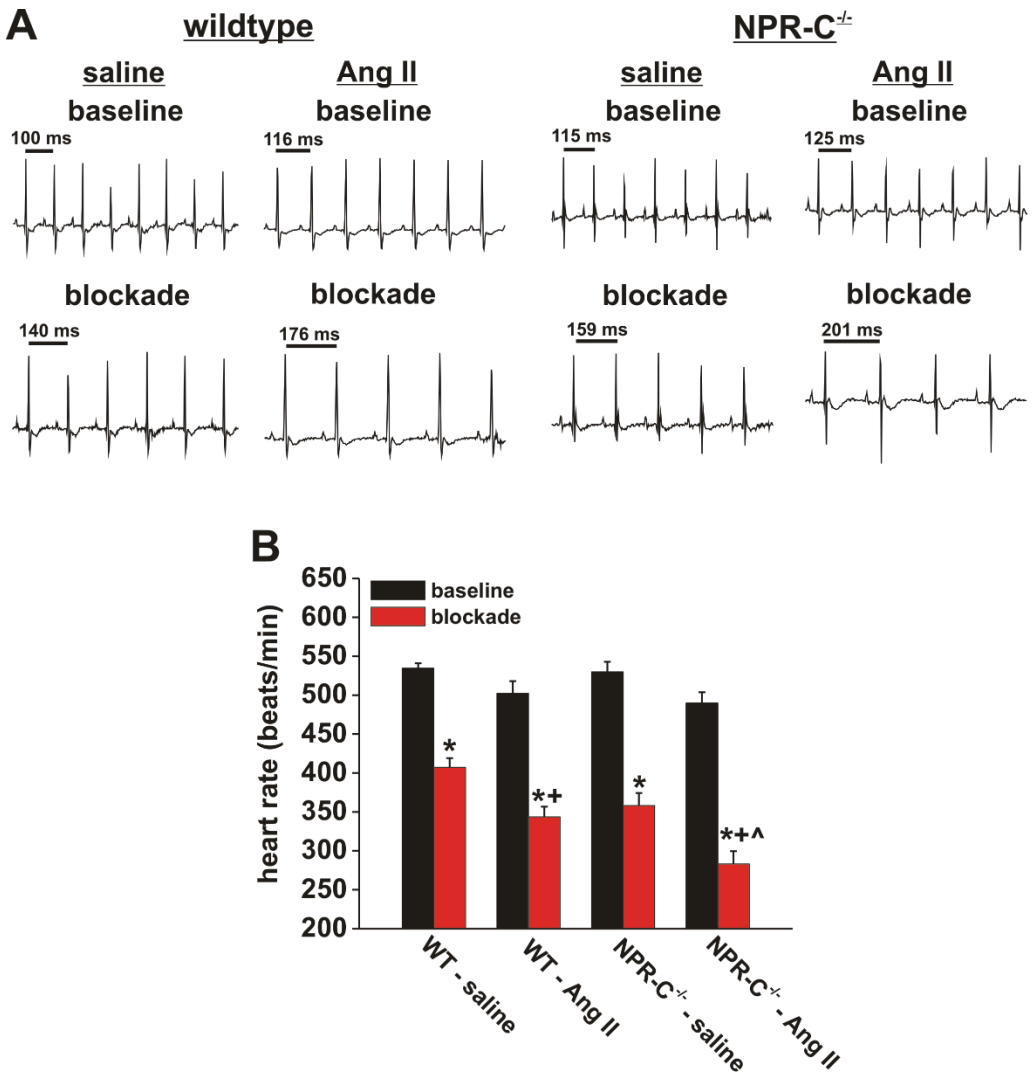

Supplemental Figure 3. Effects of autonomic nervous system blockade on heart rate in wildtype and NPR-C$^{-/-}$ mice treated with Ang II. (A) Representative ECGs in wildtype (left) and NPR-C$^{-/-}$ (right) mice treated with saline or Ang II. ECGs are shown in baseline conditions and after autonomic blockade with atropine and propranolol. **(B)** Summary data illustrating the effects of autonomic blockade in each treatment group. *P<0.001 vs. baseline within treatment group, ^{+}P=0.004 vs. saline within genotype, ^P=0.004 vs. WT-Ang II by two-way ANOVA with Tukey's post-hoc test; n=6 mice for wildtype/saline, 11 mice for wildtype/Ang II, 9 mice for NPR-C$^{-/-}$/saline and 8 mice for NPR-C$^{-/-}$/Ang II.

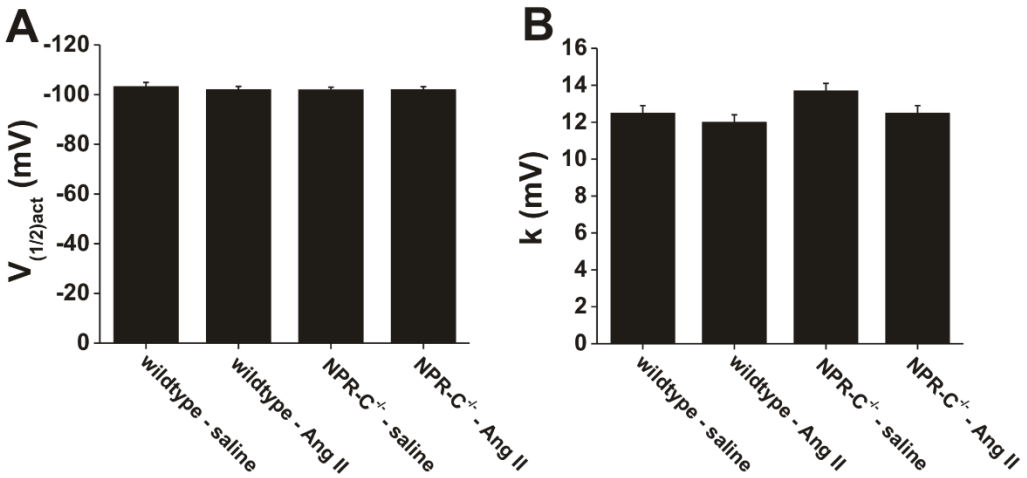

Supplemental Figure 4. I_f activation kinetics in wildtype and NPR-$C^{-/-}$ mice treated with Ang II. (A) Summary data illustrating I_f $V_{1/2(act)}$ measurements in wildtype and NPR-$C^{-/-}$ treated with saline or Ang II. There were no differences in $V_{1/2(act)}$ following Ang II treatment (*P*=0.416) or between genotypes (*P*=0.361), data analyzed by two-way ANOVA with Tukey's posthoc test. **(B)** Summary data illustrating slope factor (k) values for I_f in wildtype and NPR-$C^{-/-}$ mice treated with saline or Ang II. There were no differences in k following Ang II treatment (*P*=0.057) or between genotypes (*P*=0.061). *n*=17 cells for wildtype/saline, 13 cells for saline/Ang II; 13 cells for NPR-$C^{-/-}$/saline and 16 cells for NPR-$C^{-/-}$/Ang II.

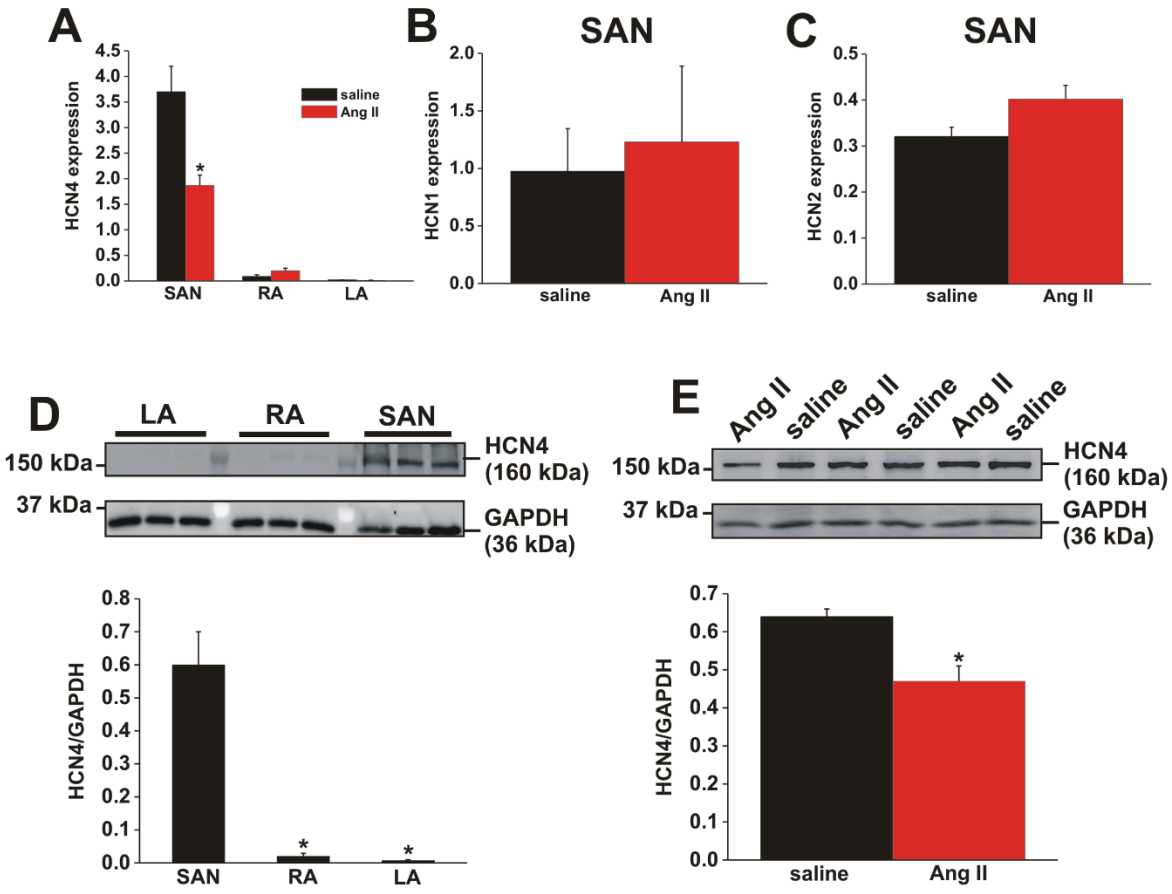

Supplemental Figure 5. Expression of HCN channels in the SAN and atria of wildtype mice treated with Ang II. (A) Expression of HCN4 mRNA in the SAN, right atrium (RA) and left atrium (LA) in saline and Ang II treated mice. **P*<0.001 vs saline by two-way ANOVA with Tukey's posthoc test; *n*=7 saline and 12 Ang II treated hearts. There was no difference in mRNA expression of HCN1 (*P*=0.517, panel **B**) or HCN2 (*P*=0.067, panel **C**) in the SAN following Ang II treatment. **(D)** Expression of HCN4 protein in SAN, RA and LA in wildtype mice. Molecular weights on the left side of the representative blot are for the molecular weight markers which can be between the LA and RA samples as well as between the RA and SAN samples. **P*=0.025 vs SAN by one way ANOVA with Tukey's posthoc test; *n*=3 for each region. **(E)** HCN4 protein expression was reduced (*P*=0.044) in the SAN following Ang II treatment. Data analyzed by Student's *t*-test; *n*=3 replicates for saline and 5 replicates for Ang II.

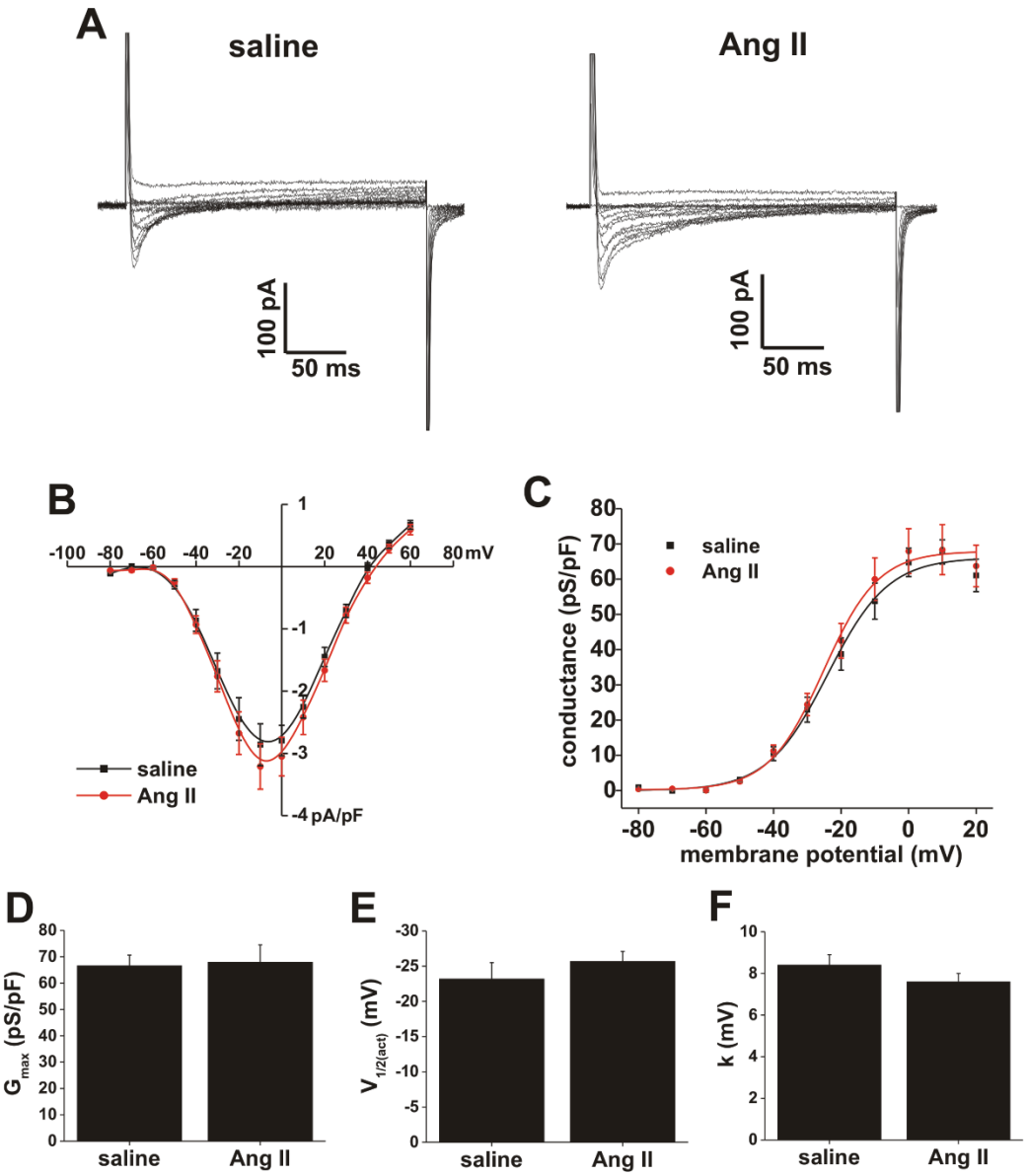

Supplemental Figure 6. Effects of Ang II on L-type Ca^{2+} current ($I_{Ca,L}$) in isolated SAN myocytes from wildtype mice. (A) Representative $I_{Ca,L}$ recordings in SAN myocytes following saline or Ang II treatment. **(B)** Summary $I_{Ca,L}$ IV curves for saline and Ang II treated SAN myocytes. There was no difference (P=0.503) in $I_{Ca,L}$ density between saline and Ang II at any membrane potential. Data analyzed by two-way repeated measures ANOVA. **(C)** $I_{Ca,L}$ activation curve for saline and Ang II treated myocytes. There were no differences in $I_{Ca,L}$ maximum conductance (G_{max}, P=0.877, panel **D**), $V_{1/2(act)}$ (P=0.342, panel **E**) or slope factor (k, P=0.270, panel **F**). Data in panels D-F analyzed by Student's t-test; n= 8 SAN myocytes for saline and 11 SAN myocytes for Ang II.

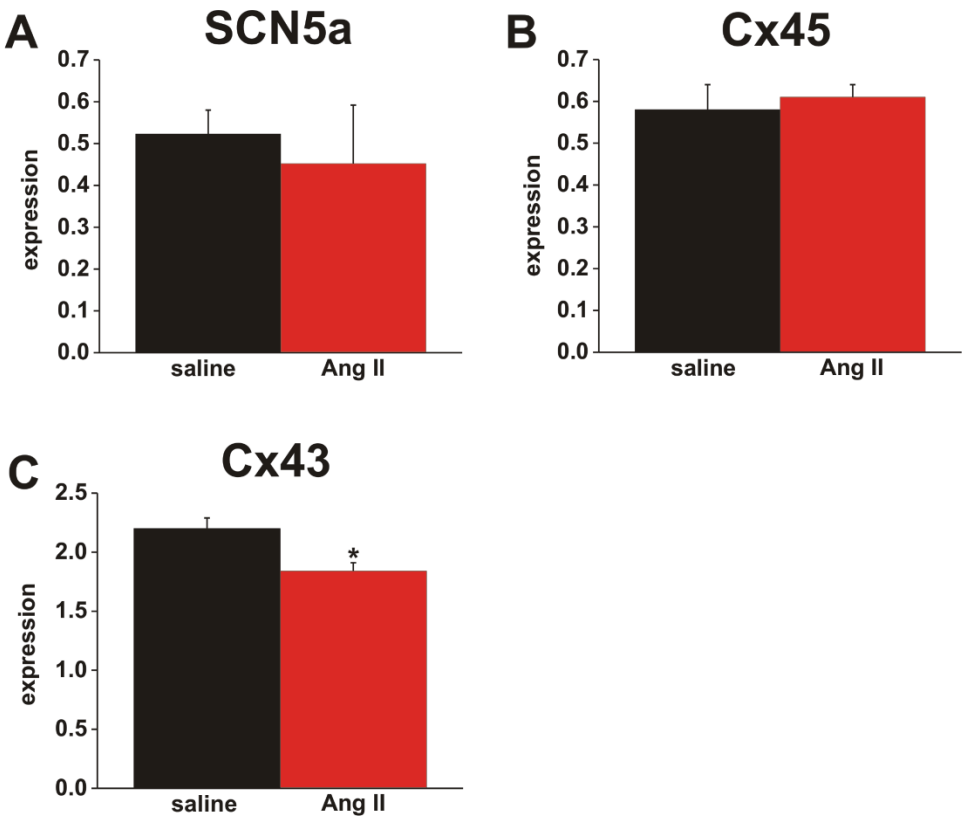

Supplemental Figure 7. Expression of SCN5a, Cx45 and Cx43 in the SAN in Ang II treated mice. (A) Summary of the mRNA expression of SCN5a in the SAN from saline and Ang II treated mice. *P*=0.335 by Student's *t*-test. **(B)** Summary of the mRNA expression of Cx45 in the SAN from saline and Ang II treated mice. *P*=0.680 by Student's *t*-test. **(C)** Summary of the mRNA expression of Cx43 in the SAN from saline and Ang II treated mice. *P*=0.002 by Student's *t*-test. For these studies *n*=7 saline and 11 Ang II treated SAN samples.

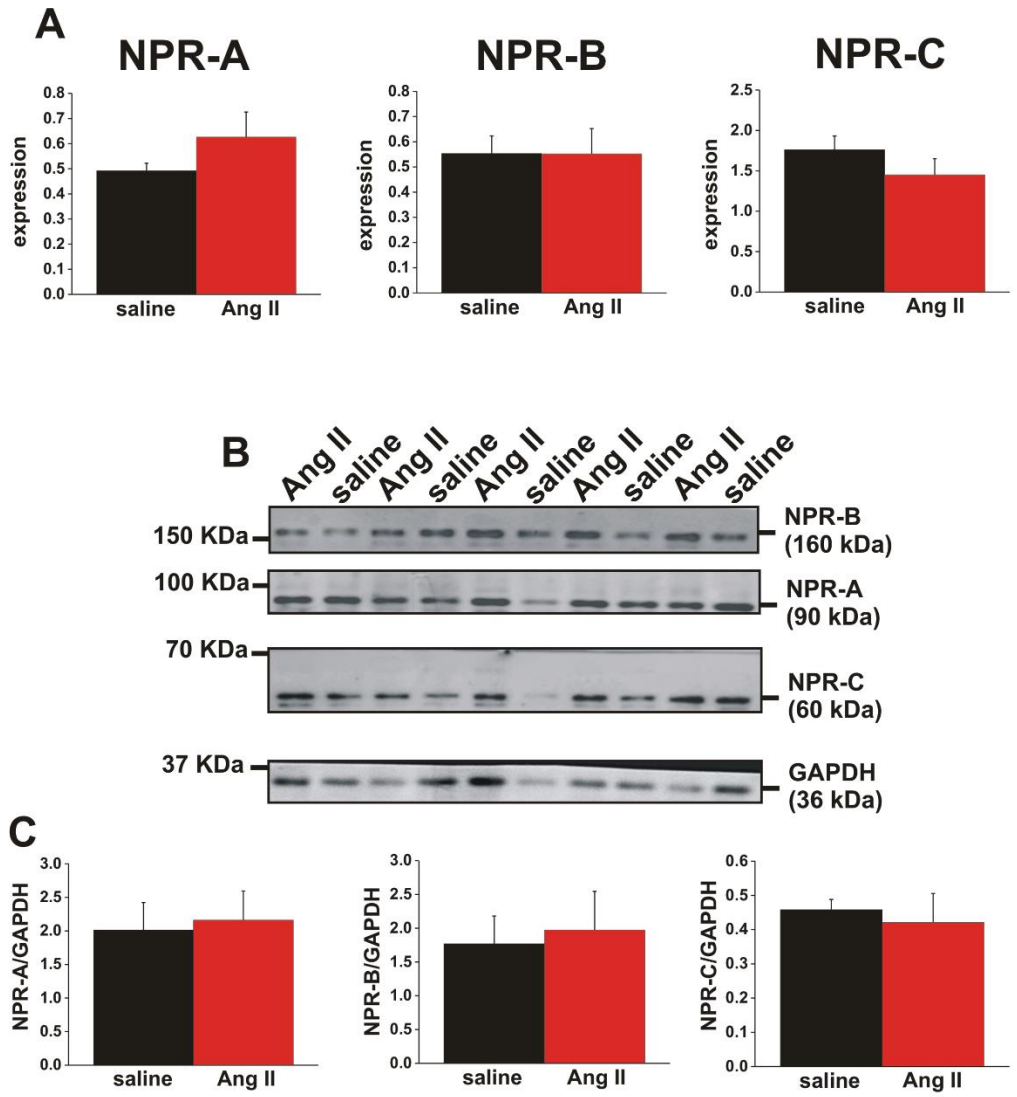

Supplemental Figure 8. Expression of natriuretic peptide receptors in the SAN of wildtype mice treated with Ang II. (A) mRNA expression of NPR-A, NPR-B and NPR-C in the SAN following saline or Ang II treatment. There was no difference in NPR-A (*P*=0.973), NPR-B (*P*=0.494) or NPR-C (*P*=0.245) expression following Ang II treatment, *n*=15 saline and 14 Ang II treated hearts, data analyzed by Student's *t*-test. **(B)** Representative Western blots for NPR-A, NPR-B and NPR-C protein expression in the SAN of wildtype mice treated with saline or Ang II. Molecular weight markers are indicated on the left side of the blot. Blots were cut at the indicated molecular weights in order to measure each protein under the same loading conditions. **(C)** Summary data showing no differences in protein expression of NPR-A (*P*=0.817), NPR-B (*P*=0.787) or NPR-C (*P*=0.699) in the SAN following Ang II treatment; *n*=3 for each treatment group, data analyzed by Student's *t*-test.

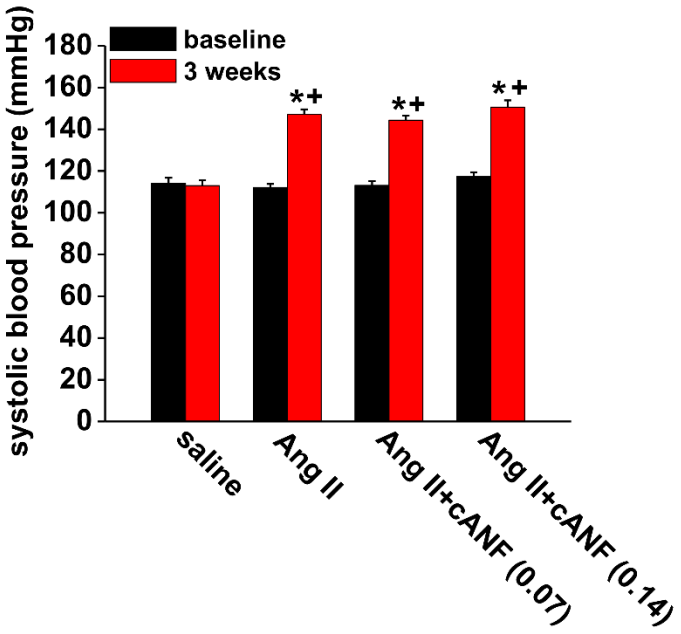

Supplemental Figure 9. Systolic blood pressure measurements in wildtype mice co-treated with Ang II and the NPR-C agonist cANF. Measurements were taken at baseline and following three weeks of treatment with saline, Ang II or Ang II + cANF (0.07 or 0.14 mg/kg/day). **P*<0.001 vs. baseline within treatment group, $^{+}$*P*<0.001 vs. saline at the 3 week time point. There were no differences in systolic blood pressure between Ang II alone and Ang II + cANF at doses of 0.07 (*P*=0.859) or 0.14 mg/kg/day (*P*=0.740) at the 3 week time point.

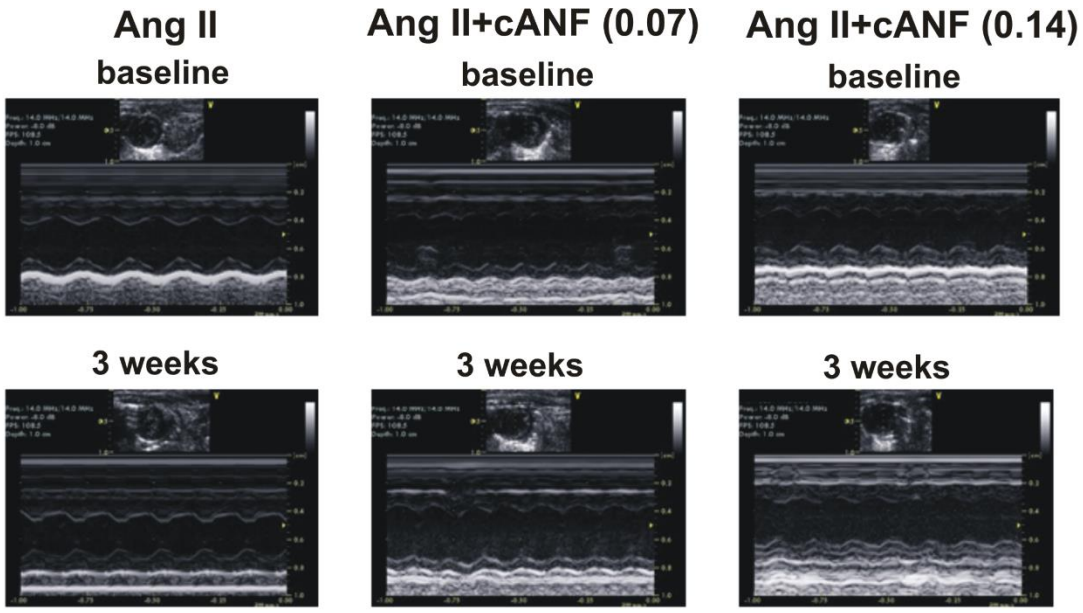

Supplemental Figure 10. Echocardiography on wildtype mice co-treated with Ang II and the NPR-C agonist cANF. M-mode imaging of the left ventricle from the parasternal short axis view at the midpapillary level at baseline and following 3 weeks of treatment with Ang II or Ang II + cANF (0.07 or 0.14 mg/kg/day). Refer to Supplemental Table 3 for summary data.

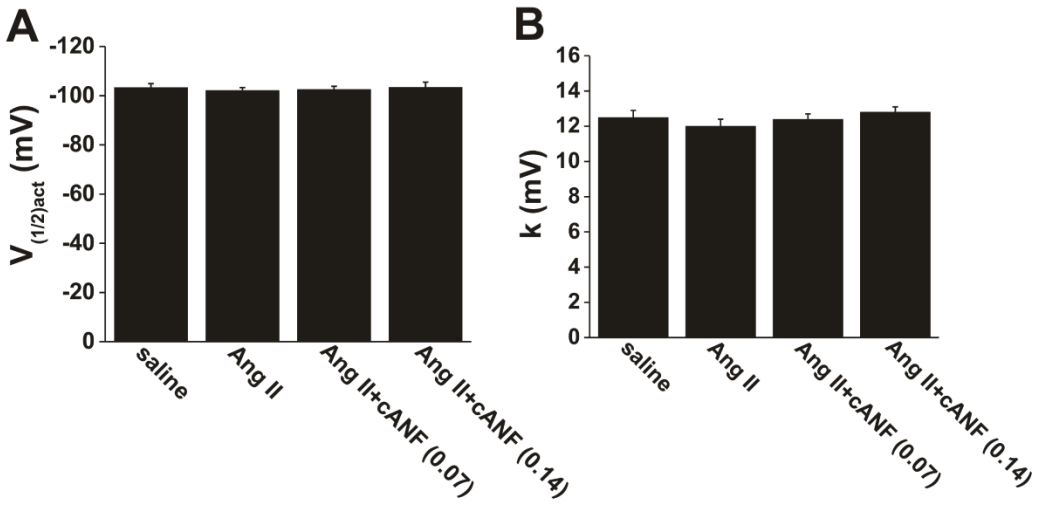

Supplemental Figure 11. I_f activation kinetics in wildtype mice co-treated with Ang II and the NPR-C agonist cANF. (A) Summary data illustrating I_f $V_{1/2(act)}$ measurements in wildtype mice treated with saline, Ang II or Ang II + cANF (0.07 or 0.14 mg/kg/day). There were no differences in $V_{1/2(act)}$ between treatment groups (*P*=0.779). **(B)** Summary data illustrating slope factor (k) values for I_f in wildtype mice treated with saline, Ang II or Ang II + cANF (0.07 or 0.14 mg/kg/day). There were no differences in k between treatment groups (*P*=0.335). Data analyzed by one-way ANOVA, *n*=17 SAN cells for saline, 13 cells for Ang II, 14 cells for Ang II + cANF (0.07) and 13 cells for Ang II + cANF (0.14).

Supplemental Table 1: Echocardiographic measurements in wildtype and NPR-C$^{-/-}$ mice treated with Ang II for 3 weeks

	Wildtype			NPR-C$^{-/-}$			
	Baseline	**Ang II (3 weeks)**	***P* value vs. baseline**	**Baseline**	**Ang II (3 weeks)**	***P* value vs. basline**	***P* value NPR-C$^{-/-}$ Ang II vs. wildtype Ang II**
IVSd (mm)	0.8±0.07	1.2±0.03*	<0.001	0.8±0.1	0.7±0.02†	0.620	<0.001
LVIDd (mm)	3.6±0.1	3.2±0.06*	0.013	3.3±0.1	4.0±0.09*†	0.002	<0.001
LVPWd (mm)	0.7±0.03	0.8±0.03	0.200	0.6±0.01	0.5±0.02†	0.250	0.036
IVSs (mm)	1.3±0.09	1.8±0.05*	0.027	1.0±0.07	1.0±0.02†	0.900	<0.001
LVIDs (mm)	2.3±0.06	1.4±0.03*	<0.001	2.8±0.12	3.2±0.03*†	0.004	<0.001
LVPWs (mm)	1.1±0.03	1.6±0.09*	0.006	0.9±0.03	0.8±0.02†	0.352	<0.001
EF (%)	64±1.2	76.3±2.4*	0.007	68.1±2.5	41.7±1.6*†	<0.001	<0.001
FS (%)	34.5±1.1	45.3±1.4*	<0.001	36.8±4.3	16.7±0.9*†	<0.001	<0.001

IVS, interventricular septum thickness; LVID, left ventricular internal diameter; LVPW, left ventricular posterior wall thickness. IVS, LVID and LVPW measurements are presented during diastole (d) and systole (s). EF, ejection fraction; FS, fractional shortening. Data are means ± SEM; *n*=10-15 mice in each group. *P<0.05 vs. baseline, $^{\dagger}P$<0.05 vs. wildtype at same time point by two way ANOVA with a Tukey posthoc test.

Supplemental Table 2: Action potential parameters in SAN myocytes from wildtype and NPR-C$^{-/-}$ mice treated with Ang II for 3 weeks

	Wildtype			**NPR-C$^{-/-}$**			
	saline	**Ang II**	***P* value vs. saline**	**saline**	**Ang II**	***P* value**	***P* value NPR-C$^{-/-}$ Ang II vs. wildtype Ang II**
n	16	12		10	13		
AP cycle length (ms)	330.5±18.5	475.1±25.5*	<0.001	348±20	481.3±14.7*	<0.001	0.557
AP frequency (APs/min)	190±11	128±6*	<0.001	179±10	126±4*	<0.001	0.435
MDP (mV)	-62.8±0.8	-62.9±0.7	0.533	-61.4±0.6	-62.5±1	0.533	0.343
DD slope (mV/s)	45.2±2.2	24±2.1*	<0.001	45.7±3.8	26.6±1.6*	<0.001	0.517
V_{max} (V/s)	14.6±8.9	15.4±10.2	0.970	12.6±9.2	14.3±8.5	0.970	0.115
OS (mV)	9.7±0.8	9.9±1.3	0.883	9.5±1.0	9.8±1.2	0.883	0.883
APD_{50} (ms)	38.7±3.8	28.7±4.6	0.162	33.5±6.8	30.6±3.4	0.162	0.713

n, sample size; MDP, maximum diastolic potential; DD slope, diastolic depolarization slope; V_{max}, maximum AP upstroke velocity; OS, overshoot; APD_{50}, AP duration at 50% repolarization; Data are means ± SEM; *P<0.05 vs. saline by two way ANOVA with a Tukey posthoc test.

Supplemental Table 3: Echocardiographic measurements in wildtype mice co-treated with Ang II and cANF for 3 weeks

	Ang II			Ang II + cANF (0.07)			Ang II + cANF (0.14)		
	Baseline	**3 weeks**	***P* value**	**Baseline**	**3 weeks**	***P* value**	**Baseline**	**3 weeks**	***P* value**
IVSd (mm)	0.8±0.07	1.2±0.03*	<0.001	0.8±0.03	1.0±0.04*	0.023	0.9±0.04	1.0±0.05	0.137
LVIDd (mm)	3.6±0.1	3.2±0.06*	0.024	3.8±0.1	3.9±0.2	0.929	3.8±0.1	3.7±0.1	0.521
LVPWd (mm)	0.7±0.03	0.8±0.03	0.004	0.7±0.03	0.8±0.06*	0.010	0.8±0.04	0.9±0.03*	0.021
IVSs (mm)	1.3±0.1	1.8±0.1*	<0.001	1.4±0.2	1.3±0.1	0.227	1.3±0.1	1.4±0.1	0.115
LVIDs (mm)	2.3±0.1	1.4±0.03*	0.004	2.8±0.1	3.0±0.2	0.253	2.7±0.1	2.8±0.2	0.545
LVPWs (mm)	1.1±0.03	1.6±0.1*	<0.001	1.0±0.05	1.1±0.05	0.143	1.2±0.08	1.2±0.06	0.870
EF (%)	64±1.2	76.3±2.4*	0.004	64.4±2.3	59.8±2.2	0.198	65.2±1.9	63.4±1.8	0.205
FS (%)	34.5±1.1	45.3±1.4*	0.002	35±1.3	31.4±1.1	0.180	31.0±1.3	29.5±1.1	0.285

The NPR-C agonist cANF was applied at 0.07 mg/kg/day or 0.14 mg/kg/day. IVS, interventricular septum thickness; LVID, left ventricular internal diameter; LVPW, left ventricular posterior wall thickness. IVS, LVID and LVPW measurements are presented during diastole (d) and systole (s). EF, ejection fraction; FS, fractional shortening. Data are means ± SEM; *n*=9-15 mice in each group. **P*<0.05 vs. baseline by one way ANOVA with a Tukey posthoc test.

Supplemental Table 4: Action potential parameters in SAN myocytes from wildtype co-treated with Ang II and cANF for 3 weeks

	Saline	Ang II	Ang II + cANF (0.07)	Ang II + cANF (0.14)	*P* value Ang II vs. saline	*P* value cANF (0.07) vs. Ang II	*P* value cANF (0.14) vs. Ang II	*P* value cANF (0.14) vs. saline
n	16	12	13	11				
AP cycle length (ms)	330.5±18.5	475.1±25.5*	415.9±19.1*†	368.4±13.3†	<0.001	0.046	0.008	0.573
AP frequency (APs/min)	190±11	128±6*	148±7*	164±6†	<0.001	0.046	0.048	0.177
MDP (mV)	-62.8±0.8	-62.9±0.7	-61.2±0.6	-61.6±1.0	0.483	0.483	0.483	0.483
DD slope (mV/s)	45.2±2.2	24±2.1*	32.2±2.5*†	40.0±1.6†^	<0.001	0.014	<0.001	0.410
V_{max} (V/s)	14.6±8.9	16.4±10.2	17.5±7	15.7±5.2	0.071	0.071	0.071	0.071
OS (mV)	9.7±0.8	9.9±1.3	9.8±1.6	8.2±1.9	0.444	0.444	0.444	0.444
APD_{50} (ms)	38.7±3.8	28.7±4.6	30.5±2.9	38.9±4.8	0.174	0.174	0.174	0.174

n, sample size; MDP, maximum diastolic potential; DD slope, diastolic depolarization slope; V_{max}, maximum AP upstroke velocity; OS, overshoot; APD_{50}, AP duration at 50% repolarization; Data are means ± SEM; **P*<0.001 vs. saline, †*P*<0.05 vs. Ang II, ^*P*=0.024 vs. Ang II + cANF (0.07) by one way ANOVA with a Tukey posthoc test.

Supplemental Table 5: Quantitative PCR primers

Gene of Interest	Forward Primer (5' → 3')	Reverse Primer (5' → 3')	Amplicon Length
NPR-A	CGAAGCTTCCAAGGTGTGACAGG	GACACAGCCATCAGCTCCTGGG	152
NPR-B	GGGGACTTTCAGCCCGCAGC	GTGGAGTTTTATCACAGGATGGGTCG	150
NPR-C	CGAGCGAGTGGTGATCATGTGTG	CTCCACGAGCCATCTCCGTAGG	147
HCN1	CTCTTTTTGCTAACGCCGAT	CATTGAAATTGTCCACCGAA	291
HCN2	CTTCACCAAGATCCTCAGTCTG	GGTCGTAGGTCATGTGGAAA	92
HCN4	CCAGGAGAAGTATAAACAGGTGGAGCG	GTTGATGATCTCCTCTCGAAGTGGCTC	169
SCN5a	GGAGTACGCCGACAAGATGT	ATCTCGGCAAAGCCTAAGGT	171
Cx45	CACTTGGAACACACCCTCTGCTC	GGGAGGTGTTCCTCGTGGCT	159
Cx43	CCAAGGAGTTCCACCACTTTG	CCATGTCTGGGCACCTCTCT	70
GAPDH	AATGGGGTGAGGCCGGTGCT	CACCCTTCAAGTGGGCCCCG	87

References

1. Springer J, Azer J, Hua R , et al. The natriuretic peptides BNP and CNP increase heart rate and electrical conduction by stimulating ionic currents in the sinoatrial node and atrial myocardium following activation of guanylyl cyclase-linked natriuretic peptide receptors. J Mol Cell Cardiol 2012;52:1122-34.
2. Egom EE, Vella K, Hua R , et al. Impaired sinoatrial node function and increased susceptibility to atrial fibrillation in mice lacking natriuretic peptide receptor C. J Physiol 2015;593:1127-46.
3. Hua R, MacLeod SL, Polina I , et al. Effects of Wild-Type and Mutant Forms of Atrial Natriuretic Peptide on Atrial Electrophysiology and Arrhythmogenesis. Circ Arrhythm Electrophysiol 2015;8:1240-54.
4. Moghtadaei M, Jansen HJ, Mackasey M , et al. The impacts of age and frailty on heart rate and sinoatrial node function. J Physiol 2016;594:7105-7126.
5. Azer J, Hua R, Krishnaswamy PS , et al. Effects of natriuretic peptides on electrical conduction in the sinoatrial node and atrial myocardium of the heart. J Physiol 2014;592:1025-45.
6. Fedorov VV, Lozinsky IT, Sosunov EA , et al. Application of blebbistatin as an excitation-contraction uncoupler for electrophysiologic study of rat and rabbit hearts. Heart Rhythm 2007;4:619-26.
7. Krishnaswamy PS, Egom EE, Moghtadaei M , et al. Altered parasympathetic nervous system regulation of the sinoatrial node in Akita diabetic mice. J Mol Cell Cardiol 2015;82:125-135.
8. Liu J, Dobrzynski H, Yanni J , et al. Organisation of the mouse sinoatrial node: structure and expression of HCN channels. Cardiovasc Res 2007;73:729-38.
9. Morley GE, Vaidya D, Samie FH , et al. Characterization of conduction in the ventricles of normal and heterozygous Cx43 knockout mice using optical mapping. J Cardiovasc Electrophysiol 1999;10:1361-75.
10. Nygren A, Lomax AE, Giles WR. Heterogeneity of action potential durations in isolated mouse left and right atria recorded using voltage-sensitive dye mapping. Am J Physiol Heart Circ Physiol 2004;287:H2634-43.
11. Mangoni ME, Couette B, Bourinet E , et al. Functional role of L-type Cav1.3 Ca2+ channels in cardiac pacemaker activity. Proc Natl Acad Sci U S A 2003;100:5543-8.
12. Zhang Z, Xu Y, Song H , et al. Functional Roles of Ca(v)1.3 (alpha(1D)) calcium channel in sinoatrial nodes: insight gained using gene-targeted null mutant mice. Circ Res 2002;90:981-7.
13. El Khoury N, Mathieu S, Marger L , et al. Upregulation of the hyperpolarization-activated current increases pacemaker activity of the sinoatrial node and heart rate during pregnancy in mice. Circulation 2013;127:2009-20.
14. Cifelli C, Rose RA, Zhang H , et al. RGS4 regulates parasympathetic signaling and heart rate control in the sinoatrial node. Circ Res 2008;103:527-35.